

# Hard exclusive production of two pions in $\gamma\gamma$ -collisions within the SCET factorization approach

---

**N. Kivel**<sup>1</sup>

*Helmholtz Institut Mainz, Johannes Gutenberg-Universität, D-55099 Mainz, Germany*  
*Institut für Kernphysik, Johannes Gutenberg-Universität, D-55099 Mainz, Germany*

**ABSTRACT:** We considered the power corrections to the amplitude describing hard exclusive pion pair production in gamma gamma collisions at large energy and momentum transfer. We showed that in order to derive a factorization formula for the subleading power corrections one has to take into account the so-called soft-overlap (or soft) contributions. These terms can be naturally introduced within the SCET framework as a matrix elements of the SCET-I operators. The so-called end-point singularities must cancel in the sum of the hard and soft contributions after matching onto SCET-II. Using the so-called physical subtraction scheme we demonstrated such cancellation in the case of twist-3 chiral enhanced contributions in the leading logarithmic approximation. As a result we obtained the well defined expression for the subleading power correction which depends only from the two unknown functions. These functions can be associated with the soft-overlap of the outgoing pion state and therefore does not depend on the scattering angle. The angular dependence in this case is defined by the hard subprocess and can be computed in a model independent way.

The obtained results were used in the phenomenological analysis of existing data. We showed that using the leading and subleading contributions and considering the unknown functions as a free parameters one can describe consistently the data for  $\pi^+\pi^-$  and  $\pi^0\pi^0$  production. The soft-overlap corrections play an important role in order to achieve the agreement with the data. In order to understand better the dynamics of the production mechanism we suggested to perform an additional independent measurement of the combination of the hadronic cross sections in the  $e^+e^-$  scattering. With the help of this data one can better discriminate between the different theoretical models for the hard exclusive pion production.

---

<sup>1</sup> On leave of absence from St. Petersburg Nuclear Physics Institute, 188350, Gatchina, Russia

---

## Contents

<b>1</b>	<b>Introduction</b>	<b>1</b>
<b>2</b>	<b>General information about the process <math>\gamma\gamma \rightarrow \pi\pi</math></b>	<b>5</b>
2.1	Kinematics, amplitudes and cross sections	5
2.2	Leading twist results	7
<b>3</b>	<b>Factorization of the subleading amplitudes in SCET</b>	<b>10</b>
3.1	Soft Collinear Effective Theory approach: general remarks	10
3.2	Analysis of the subleading power contributions in SCET	14
<b>4</b>	<b>Calculation of the leading-order coefficient functions for the power sub-leading contributions</b>	<b>26</b>
4.1	The soft contribution	26
4.2	The subleading hard contribution	28
4.3	Subleading amplitudes in the physical subtraction scheme	29
<b>5</b>	<b>Phenomenological analysis</b>	<b>32</b>
5.1	Analysis of BELLE data using the BA-model of pion DA	34
5.2	Analysis of BELLE data using the CZ-model of pion DA	39
<b>6</b>	<b>Discussion</b>	<b>42</b>
<b>A</b>	<b>Higher twist pion distribution amplitudes</b>	<b>44</b>

---

## 1 Introduction

Hard exclusive reactions provide us an important information about nonperturbative characteristics of the hadronic states which can not be accessed in inclusive processes. The two-photon production of hadronic states are considered as the one of the most attractive exclusive channel because the colliding photons provide a cleanest possibility to study the complicate hadronic formation dynamics. From the experimental point of view such reactions can be studied in  $e^+e^-$  colliders and general formalism which allows one to extract the hadronic cross sections has been developed in details already long time ago in Ref.[1]. The processes with large angle meson production  $\gamma\gamma \rightarrow MM$  can be considered as one of the most interesting example of such hadronic reactions. In this case the amplitude of the process can be computed in the framework of QCD factorization approach. The unknown nonperturbative matrix elements are related to the properties of meson wave functions. The nice feature of the QCD factorization is that this nonperturbative functions are universal, i.e. their definition is process independent. Therefore they can be constrained using

information from the different hadronic reactions. Hence the analysis of hard exclusive meson production allows one to obtain an important information about nonperturbative hadronic input which then can be also used to study the other hard reactions.

The factorization theorem for large angle pair production of mesons have been suggested long time ago in Ref.[2]. In this case the amplitude of the process is given by the convolution integral of the hard kernel with the light-cone distribution amplitude (DA). The hard kernel or the coefficient function describes the hard subprocess  $\gamma\gamma \rightarrow \bar{q}q + \bar{q}q$  and can be computed systematically in perturbation theory order by order. The DA describes the nonperturbative overlap of the two quarks with the meson and can not be computed from the first principles.

The interesting case of the hadron pair production is given by the process  $\gamma\gamma \rightarrow \pi^+\pi^-$  in the region where  $s \sim -t \sim -u \gg \Lambda_{QCD}^2$ . The asymptotic behavior of the cross section was obtained in Ref.[2] using factorization approach

$$\frac{d\sigma^{\gamma\gamma \rightarrow \pi\pi}}{d\cos\theta} \sim \frac{f_\pi^4}{s^3} \frac{1}{\sin^4\theta}. \quad (1.1)$$

Here  $\theta$  is the scattering angle in the center-of-mass frame,  $f_\pi = 131\text{MeV}$  is the pion decay constant. A comprehensive phenomenological analysis of this reaction was also carried out in Ref.[3].

The cross section of hard exclusive  $\pi^+\pi^-$ -production was measured at sufficiently large energy in the several experiments, see e.g. CLEO [4] and ALEPH [5]. The most precise measurements of the cross sections for charged and neutral pion pairs production in the region up to  $\sqrt{s} = 4\text{GeV}$  were performed by BELLE collaboration [6, 7], see also review [8]. The analysis of the experimental data shows that the theoretical estimates obtained in within the factorization framework describe reasonably well the angular behavior of the cross sections but underestimate their the absolute value, see e.g. [9]. Especially the significant discrepancy between the theory and experiment was observed for the neutral pion channel.

In order to explain such situation within the QCD factorization picture it is suggested to use a specific model for the pion distribution amplitude (DA) which describes the nonperturbative input. With this model the realistic virtualities of the hard particles are assumed to be much smaller then the large external kinematical variables and therefore one can fix the relatively large value of the QCD coupling  $\alpha_s \simeq 0.4$ , see e.g. Refs. [3, 10, 11]. Such approach allows one to reach a certain qualitative agreement with the  $\pi^+\pi^-$  data but can not still explain the discrepancy in the  $\pi^0\pi^0$  channel. In [11] it is proposed that the large contribution in this channel can arise at higher orders in  $\alpha_s$  due to the specific three gluon exchange diagrams.

The other scenario which can also explain the mismatch of the leading-order pQCD predictions and experimental data implies a different idea about the underlying QCD dynamics. It is assumed that the leading order contribution obtained in the framework of QCD factorization becomes dominant only at very large asymptotical energies which are considerably larger then the energy values relevant for the current experiments. Such scenario also implies the different shape of the pion DA and as a result relatively small value of

the cross section computed at the leading-order approximation. Corresponding model for the pion DA is obtained from the other processes, like  $\gamma^*\gamma \rightarrow \pi^0$  or pion electromagnetic form factor computed in the QCD sum rule technique, see e.g. [12–16] and references therein. In this case the discrepancy can be explained by the large numerical effect provided by subleading power corrections. A bulk of this effect is associated with the so-called soft-overlap or the same Feynman mechanism. Such configuration describes the soft-overlap of the hadronic states and arises only as a power correction to the leading asymptotic contribution in Eq.(1.1). Nevertheless it was found that numerically this contribution is large and even dominant at moderate values of the hard scale  $Q$ . The soft-overlap contribution can be especially important if the leading order term is already of order  $\alpha_s$  and therefore is suppressed numerically.

This idea was applied for the description of the large angle processes  $\gamma\gamma \rightarrow MM$  in the framework of the so-called handbag model in Refs.[17, 18]. In this model the soft-overlap contribution is described by the two-pion matrix element which is associated with the two-pion distribution amplitude. The important moment is that this function depends only from the total energy  $s$ . This allows one to compute the scattering angle behavior which is defined only by the hard subprocess. In Ref.[17] it was obtained that this model also provides a  $1/\sin^4\theta$  behavior for the pion cross sections as the leading power term in Eq.(1.1). The unknown two-pion distribution amplitude describing the soft-overlap of the pions was fitted from the data. Therefore this allows one to describe the data using assumption about the large soft-overlap contribution. The important moment is that this approach automatically gives a large value of the problematic  $\pi^0\pi^0$  cross section providing that the ratio  $R = d\sigma^{\pi^0\pi^0}/d\sigma^{\pi^+\pi^-} = 1/2$ . This result is somewhat larger than the experimental value  $R_{exp} = 0.32 \pm 0.03$  extracted in the region where  $\sqrt{s} = 3.1 - 4.1\text{GeV}$  [7].

Despite interesting discussion and results this handbag model has many problematic points which have to be better understood. Some critical remarks were considered in Refs. [10, 11]. The most important problem is to provide a consistent and clear formulation of the soft-overlap contribution in order to implement it into the theoretical description and to avoid a double counting with the power corrections arising also from the hard power suppressed configurations. Having such a framework allows one to reduce the model dependence of the theoretical description to a minimum. Motivated by this challenge we try to develop such approach in present paper.

The main our task is to extend the QCD factorization approach beyond the leading power approximation. Such an extension can not be done only by computation of the subleading hard contributions. It is well known that such corrections are even not well defined because the convolution integrals with the higher twist DAs have the so-called end-point divergencies. These singularities appear due to the overlap of the collinear and soft regions and also known in the literature as rapidity divergencies. The soft-overlap contribution in this case can be associated with the soft region. In order to describe such configuration one has to deal with the effective field theory which takes into account the soft and collinear modes. Such effective theory was built some time ago and known as soft collinear effective theory (SCET), see e.g. [19–24]. Using this approach one can try

to define the soft-overlap contribution as an matrix element of some operators within the SCET framework.

In SCET the factorization can be carried out in two steps: first, one perform the factorization of the hard modes ( particles with momenta  $p_\mu \sim Q$ ) and passes from the full QCD to the effective theory SCET-I. This theory includes the collinear, hard-collinear and soft degrees of freedom. One can factorize the hard-collinear modes which describe particles with the virtualities  $p_{hc}^2 \sim Q\Lambda$ , where the  $\Lambda$  is generic soft scale of order  $\Lambda_{QCD}$ . The second factorization is possible if the hard scale  $Q$  is sufficiently large so that the hard-collinear scale  $\mu_{hc}^2 \sim Q\Lambda$  is a good expansion parameter in pQCD. Integrating out the hard-collinear particles one obtains the effective theory with the soft and collinear particles which is also called SCET-II.

Within this scheme the *moderate* values of  $Q^2$  can be defined as a region where the hard-collinear scale is still relatively small  $\mu_{hc}^2 \leq 1 - 1.5\text{GeV}^2$  and the factorization of the hard-collinear contributions can not provide a good approximation. The kinematical region relevant for existing experiments corresponds to  $\sqrt{s} = 3 - 4\text{GeV}$ . ne easily obtain that in this region the hard-collinear scale is not large  $\mu_{hc}^2 \sim 1.2 - 1.6\text{GeV}^2$  where we used  $\Lambda \simeq 400\text{MeV}$ . In addition the values of the momentum transfer  $-t$  in the region with  $\cos\theta < 0.6$  are even smaller and therefore the corresponding hard-collinear particles have much smaller virtualities then it was estimated above. Hence in this region one can only factorize the hard modes. Therefore the expected expression for the amplitude can include the matrix elements from all possible operators defined in SCET-I. These operators can be naturally associated with the hard and soft contributions.

The factorization of the soft terms in SCET-II involves the operators which are built only from the soft fields and therefore these terms can be associated with the soft-overlap contributions. Such a formal scheme is not complete because one must also define the specific regularization scheme for rapidity integrals in order to avoid the end-point divergencies and to define the factorization of the collinear and soft regions unambiguously. In some cases this problem can be solved using the the so-called physical subtraction scheme which allows one to express the SCET-I soft contribution in terms of physical amplitudes or form factors. In the given paper we will use the described sSCET factorization scheme in order to construct the factorization of the subleading power contribution to the amplitudes describing the process  $\gamma\gamma \rightarrow \pi\pi$ .

Our paper is organized as follows. In section 2 we specify notation and kinematics and briefly review the leading twist results. In section 3 we perform the analysis of the relevant subleading SCET-I operators and discuss the overlap of the hard and soft contributions. Using these results we derive the factorization formula which takes into account power corrections of order  $1/Q$  and  $1/Q^2$  with respect to the leading-order contribution. We show that this formula includes the operators which define the soft and hard power suppressed contributions. Corresponding operators can mix in SCET-II due to the overlap of the collinear and soft regions. We explain how to define the physical subtraction scheme in order to avoid the problem with the end-point singularities in the hard subleading terms. In section 4 we compute the relevant hard-coefficient functions at the leading-order and derive the well defined expressions for the physical amplitudes. Section 5 is devoted to

the phenomenological analysis. We compare the obtained results with BELLE data and consider the different scenarios which associated with the different models of the pion DA. The summary of our results and conclusions is presented in section 6. In Appendix A we provide an additional useful information about the higher twist distribution amplitudes of pion.

## 2 General information about the process $\gamma\gamma \rightarrow \pi\pi$

### 2.1 Kinematics, amplitudes and cross sections

In order to describe the process  $\gamma(q_1)\gamma(q_2) \rightarrow \pi(p)\pi(p')$  we choose center-of-mass system (c.m.s.)  $\mathbf{p} + \mathbf{p}' = 0$  with the pion momenta directed along  $z$ -axis. We define the Mandelstam variables as

$$s = (q_1 + q_2)^2 \equiv W^2, \quad t = (p - q_1)^2, \quad u = (p - q_2)^2, \quad (2.1)$$

In c.m.s. the particle momenta read

$$p = \frac{W}{2}(1, 0, 0, \beta), \quad p' = \frac{W}{2}(1, 0, 0, -\beta), \quad (2.2)$$

$$q_1 = \frac{W}{2}(1, \sin\theta, 0, \cos\theta), \quad q_2 = \frac{W}{2}(1, -\sin\theta, 0, -\cos\theta), \quad (2.3)$$

where  $\theta$  is the scattering angle and  $\beta$  is the pion velocity

$$\beta = \sqrt{1 - \frac{4m_\pi^2}{s}}. \quad (2.4)$$

We will also use the auxiliary light-cone vectors

$$n = (1, 0, 0, -1), \quad \bar{n} = (1, 0, 0, 1), \quad (n \cdot \bar{n}) = 2. \quad (2.5)$$

In this paper we consider the kinematical region where  $s \sim -t \sim -u \gg m_\pi^2$  therefore we neglect the pion mass. Then the light-cone decomposition of the momenta read

$$p \simeq W \frac{\bar{n}}{2}, \quad p' \simeq W \frac{n}{2}, \quad (2.6)$$

$$q_1 = \frac{(1 - \cos\theta)}{2} W \frac{n}{2} + \frac{(1 + \cos\theta)}{2} W \frac{\bar{n}}{2} + q_\perp, \quad (2.7)$$

$$q_2 = \frac{(1 + \cos\theta)}{2} W \frac{n}{2} + \frac{(1 - \cos\theta)}{2} W \frac{\bar{n}}{2} - q_\perp, \quad (2.8)$$

with

$$q_\perp^2 = \frac{s}{4}(1 - \cos^2\theta). \quad (2.9)$$

The process  $\gamma\gamma \rightarrow \pi\pi$  is described by the matrix element

$$\langle \pi^{+/0}(p), \pi^{-/0}(p') \text{ out} | \gamma(q_1)\gamma(q_2) \text{ in} \rangle = i(2\pi)^4 \delta(p_1 + p_2 - q_1 - q_2) M_{\gamma\gamma \rightarrow \pi\pi}, \quad (2.10)$$

where the amplitude

$$M_{\gamma\gamma \rightarrow \pi\pi} = e^2 \varepsilon_\mu(q_1) \varepsilon_\nu(q_2) M_{\gamma\gamma \rightarrow \pi\pi}^{\mu\nu}, \quad (2.11)$$

with the following hadronic tensor

$$M_{\gamma\gamma\rightarrow\pi\pi}^{\mu\nu} = i \int d^4x e^{-i(q_1x)} \left\langle \pi^{+/0}(p), \pi^{-/0}(p') \mid T\{ J_{\text{em}}^\mu(x), J_{\text{em}}^\nu(0) \} \mid 0 \right\rangle. \quad (2.12)$$

Here  $J_{\text{em}}^\mu$  denotes the electromagnetic current and  $e^2 = 4\pi\alpha \simeq 4\pi/137$ . It is convenient to pass to the pion isotopic coordinates  $(\pi^\pm, \pi^0) \rightarrow (\pi^1, \pi^2, \pi^3)$  and consider the matrix element describing the process  $\gamma\gamma \rightarrow \pi^a \pi^b$  introducing

$$T_{ab}^{\mu\nu} = i \int d^4x e^{-i(q_1x)} \left\langle \pi^a(p), \pi^b(p') \mid T\{ J_{\text{em}}^\mu(x), J_{\text{em}}^\nu(0) \} \mid 0 \right\rangle, \quad (2.13)$$

This amplitude can be parametrized as, see e.g. Ref.[25]

$$\begin{aligned} T_{ab}^{\mu\nu} = & M_{++}^{\mu\nu} \left\{ \delta^{ab} T_{++}^{(0)}(s, t) + \delta^{a3} \delta^{b3} T_{++}^{(3)}(s, t) \right\} \\ & + M_{+-}^{\mu\nu} \left\{ \delta^{ab} T_{+-}^{(0)}(s, t) + \delta^{a3} \delta^{b3} T_{+-}^{(3)}(s, t) \right\} + \dots, \end{aligned} \quad (2.14)$$

where dots denote the additional structures which vanish when contracted with the photon polarization vectors. The two Lorentz tensors in Eq.(2.14) read

$$M_{++}^{\mu\nu} = \frac{1}{2} g^{\mu\nu} - \frac{1}{s} q_1^\nu q_2^\mu, \quad (2.15)$$

$$M_{+-}^{\mu\nu} = \frac{1}{2} g^{\mu\nu} + \frac{s}{4tu} \left\{ \Delta^{\mu\nu} - q_1^\nu q_2^\mu - \frac{\nu}{s} (q_1^\nu \Delta^\mu - q_2^\mu \Delta^\nu) \right\}, \quad (2.16)$$

where we defined  $\nu = t - u = -2(q_1 \cdot \Delta)$  and  $\Delta = p_1 - p_2$ . The two tensor structures  $M_{\pm\pm}^{\mu\nu}$  describe the appropriate photon helicity amplitudes  $M_{\lambda_1\lambda_2}$  and satisfy following relations<sup>1</sup>

$$q_1^\mu M_{+\pm}^{\mu\nu} = q_2^\nu M_{+\pm}^{\mu\nu} = 0, \quad M_{++}^{\mu\nu} M_{+-}^{\mu\nu} = 0, \quad M_i^{\mu\nu} M_i^{\mu\nu} = \frac{1}{2}. \quad (2.17)$$

The amplitudes  $T_{\pm\pm}^{(0,3)}$  are symmetric under crossing  $(t, u) \rightarrow (u, t)$ . The produced two-pion state is  $C$ -even and can be decomposed into isotopic amplitudes with the isospin  $I = 0, 2$ . For the physical pion states the amplitudes defined in Eq.(2.14) read

$$M_{\gamma\gamma\rightarrow\pi^+\pi^-}^{\mu\nu} = M_{++}^{\mu\nu} T_{++}^{(0)} + M_{+-}^{\mu\nu} T_{+-}^{(0)}, \quad (2.18)$$

$$M_{\gamma\gamma\rightarrow\pi^0\pi^0}^{\mu\nu} = M_{++}^{\mu\nu} (T_{++}^{(0)} + T_{++}^{(3)}) + M_{+-}^{\mu\nu} (T_{+-}^{(0)} + T_{+-}^{(3)}). \quad (2.19)$$

Corresponding cross sections read ( remind that we neglected pion mass)

$$\frac{d\sigma^{\pi^+\pi^-}}{d\cos\theta} = \frac{\pi\alpha^2}{16s} \left( |T_{++}^{(0)}|^2 + |T_{+-}^{(0)}|^2 \right), \quad (2.20)$$

$$\frac{d\sigma^{\pi^0\pi^0}}{d\cos\theta} = \frac{\pi\alpha^2}{32s} \left( |T_{++}^{(0)} + T_{++}^{(3)}|^2 + |T_{+-}^{(0)} + T_{+-}^{(3)}|^2 \right). \quad (2.21)$$

---

<sup>1</sup>Usually one defines four helicity amplitudes  $M_{++}$ ,  $M_{--}$ ,  $M_{+-}$  and  $M_{-+}$ . However for the pion production  $M_{++} = M_{--}$  and  $M_{+-} = M_{-+}$  and for brevity we do not write  $M_{--}$  and  $M_{-+}$ .

## 2.2 Leading twist results

In the limit of large energy and momentum transfer  $s \sim -t \sim -u \gg \Lambda_{\text{QCD}}$  one can describe the asymptotic behavior of the production amplitudes using factorization approach, see e.g. Ref.[2] and reviews in Refs.[26, 27]. Let us briefly review the obtained results. We rewrite the amplitude as

$$T_{+\pm}^{(i)} = A_{+\pm}^{(i)} + B_{+\pm}^{(i)}, \quad (2.22)$$

where  $A_{+\pm}^{(i)}$  and  $B_{+\pm}^{(i)}$  denote the leading and subleading power (or twist) contributions, respectively. The leading-twist leading-order contributions are given by one gluon exchange diagrams as in Fig.1.

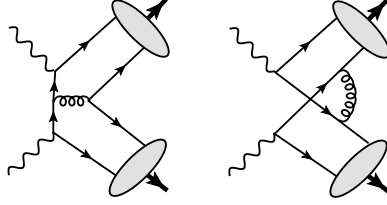


**Figure 1.** Example of the leading-twist leading-order in  $\alpha_s$  contribution to the large-angle two pion production in the  $\gamma\gamma$  collisions. The shaded blobs denote the pion DAs.

In this case the nonperturbative dynamics is described by the twist-2 pion distribution amplitude (DA) which is defined as a following matrix element

$$f_\pi \varphi_\pi(x) = i \int_{-\infty}^{\infty} \frac{d\lambda}{\pi} e^{-i(2x-1)(p' \cdot \bar{n})} \lambda \langle \pi^-(p') | \bar{d}(\lambda \bar{n}) \not{n} \gamma_5 u(-\lambda \bar{n}) | 0 \rangle. \quad (2.23)$$

with the pion decay constant  $f_\pi = 131 \text{ MeV}$ . This definition implies that

$$\int_0^1 dx \varphi_\pi(x) = 1. \quad (2.24)$$

Corresponding coefficient functions have been computed in Ref.[2]. These results can be represented as

$$A_{++}^{(0)} = -A_{++}^{(3)} = -\frac{(4\pi f_\pi)^2}{s} \frac{\alpha_s}{\pi} \frac{C_F}{N_c} \frac{1}{1 - \cos^2 \theta} \left\langle \frac{1}{x} \right\rangle^2, \quad (2.25)$$

$$A_{+-}^{(0)} = -\frac{(4\pi f_\pi)^2}{s} \frac{\alpha_s(\mu_R)}{\pi} \frac{C_F}{N_c} \left\{ \frac{1}{1 - \cos^2 \theta} \left\langle \frac{1}{x} \right\rangle^2 - \frac{1}{9} J(\theta) \right\} \quad (2.26)$$

$$A_{+-}^{(3)} = \frac{(4\pi f_\pi)^2}{s} \frac{\alpha_s(\mu_R)}{\pi} \frac{C_F}{N_c} \left\{ \frac{1}{1 - \cos^2 \theta} \left\langle \frac{1}{x} \right\rangle^2 - \frac{1}{4} J(\theta) \right\}. \quad (2.27)$$

In these equations we used that the pion DA is symmetrical function with respect to exchange  $x \leftrightarrow 1-x$ :  $\varphi_\pi(1-x) = \varphi_\pi(x)$ . We also used the standard definitions  $C_F = \frac{N_c^2 - 1}{2N_c}$ ,  $\alpha_s$  is the QCD running coupling defined at some scale  $\mu_R \sim Q$ . We used the short notation for the convolution integrals

$$\left\langle \frac{1}{x} \right\rangle = \int_0^1 dx \frac{\varphi_\pi(x)}{x}, \quad (2.28)$$



and

$$J(\theta) = \int_0^1 dx \int_0^1 dy \frac{1}{x\bar{x}} \frac{1}{y\bar{y}} \frac{(\bar{x}\bar{y} + xy)(x\bar{x} + y\bar{y})}{(\bar{x}\bar{y} + xy)^2 - (\bar{x}\bar{y} - xy)^2 \cos^2 \theta}, \quad \bar{x} \equiv 1 - x. \quad (2.29)$$

Using Eqs.(2.18) and (2.19) one easily finds the physical amplitudes. For the  $\pi^0\pi^0$  production one obtains

$$A_{++}^{(0)} + A_{++}^{(3)} = \mathcal{O}(\alpha_s^2), \quad (2.30)$$

$$A_{+-}^{(0)} + A_{+-}^{(3)} = -\frac{(4\pi f_\pi)^2}{s} \frac{\alpha_s}{\pi} \frac{C_F}{N_c} \frac{5}{36} J(\theta). \quad (2.31)$$

Notice that the integral  $J(\theta)$  is real and therefore all the leading twist amplitudes at leading-order are real. This can be explained by the absence of any  $s$ -channel cut in the leading-order diagrams.

The phenomenological analysis based on the leading twist formulas (2.25)-(2.27) has been discussed in Ref.[3]. Here we briefly discuss the numerical estimates for the pion production cross sections. In order to apply the leading twist description one has to fix a model for the pion DA. Following to a standard approach we present these function as the following decomposition

$$\varphi_\pi(x) = 6x\bar{x} \sum_n a_{2n}(\mu_F) C_{2n}^{3/2}(2x-1). \quad (2.32)$$

The coefficients  $a_{2n}$  defined in this equation are multiplicatively renormalizable at leading logarithmic approximation. We consider the models with following set of parameters  $a_{2n}$ :

$$\text{set-I: } \mu_F = 1\text{GeV}, \quad a_0 = 1, \quad a_2 = 0.25, \quad a_{2n} = 0, \quad n > 2. \quad (2.33)$$

This model is often used in literature as some realistic approximation of pion DA. The following two models

$$\begin{aligned} \text{set-BA: } \mu_F = 1\text{GeV}, \quad a_0 = 1, \quad a_2 = a_4 = a_6 = 0.1, \\ a_8 = 0.034, \quad a_{2n} = 0, \quad n > 8, \end{aligned} \quad (2.34)$$

$$\begin{aligned} \text{set-BMS: } \mu_F = 2.4\text{GeV}, \quad a_0 = 1, \quad a_2 = 0.157, \quad a_4 = -0.192, \quad a_6 = 0.226, \\ a_{2n} = 0, \quad n > 4, \end{aligned} \quad (2.35)$$

have been recently suggested in Refs. [13] and [15], respectively. The alternative popular estimate was suggested in [33]

$$\text{set-CZ: } \mu = 1\text{GeV}, \quad a_0 = 1, \quad a_2 = 2/3, \quad a_{2n} = 0, \quad n > 2, \quad (2.36)$$

The normalization scale for the running coupling we fix to be  $\mu_R = 0.8W\text{GeV}$  for the models defined as set-I,BA,BMS. For CZ-model we will use  $\mu_R = 1.3\text{GeV}$  as in Ref.[3]. The inverse Mellin moment defined in Eq. (2.28) can be represented as

$$\left\langle \frac{1}{x} \right\rangle = 3(1 + a_2 + a_4 + \dots + a_{2n} + \dots). \quad (2.37)$$

Then for the different models described above one obtains ( $\mu_F = 1\text{GeV}$ )

$$\left\langle \frac{1}{x} \right\rangle_I = 3.75, \quad \left\langle \frac{1}{x} \right\rangle_{\text{BA}} = 4.00, \quad \left\langle \frac{1}{x} \right\rangle_{\text{BMS}} = 4.05, \quad \left\langle \frac{1}{x} \right\rangle_{\text{CZ}} = 5. \quad (2.38)$$

The integral  $J(\theta)$  defined in Eq.(2.29) will be computed numerically. In Refs. [2, 3] it as found that this integral provides relatively small numerical effect. Therefore the main difference between the different models of pion DA is provided by the inverse moments (2.38) and by the scale setting for the running coupling  $\alpha_s$ .

For simplicity, we also neglect the imaginary parts which can arise in the timelike kinematics from the evolution logarithms of the DAs. Such effect can be relevant for the diagrams where photons couple to the same quark and the virtuality of the gluon propagator is positive ( $\sim s$ ). However in the diagrams where the photons couple to quark and antiquark the virtuality of the gluon propagator is negative ( $\sim -t$  or  $-u$ ). Such difference is obviously related with the presence of the different scales: positive scale  $s$  and negative  $t < 0$  and  $u < 0$ . Therefore one has to be careful with definition of running coupling for different cases because in the timelike region one has to care about resummation of large- $\pi$  contributions, see e.g. Ref.[34]. In our estimates we do not consider these effects and use  $\alpha_s$  defined at some spacelike scale.

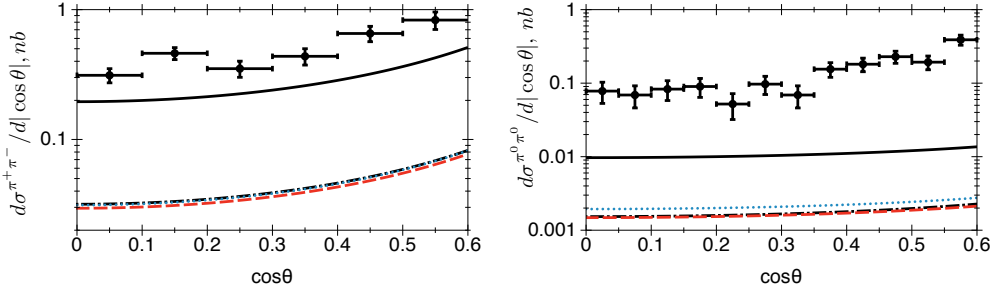


**Figure 2.** The differential cross sections as a function of  $\cos \theta$  at the leading twist approximation at  $W = 3.05\text{GeV}$ . The black solid line corresponds CZ-model, red dashed curve describes set-I model, black dot-dashed and blue dotted curves describe BA and BMS models respectively. The data are from Ref.[6, 7]

In Fig.2 we show the comparison of the leading twist estimates for differential cross sections at  $W = 3.05\text{GeV}$  in comparison with the BELLE data [6, 7]. For all models except CZ we used  $\mu_R = 2.4\text{GeV}$ . The relatively low value of the renormalization scale  $\mu_R = 1.3\text{GeV}$  is fixed for the case of CZ-model that yields  $\alpha_s(1.7\text{GeV}^2) = 0.395$ . Such a choice for is dictated by the important role of the end-point region  $x \sim 1$  or  $x \sim 0$  for the CZ-model of DA. In this region the virtuality of the hard gluon is relatively small and therefore this dictates such a small value of  $\mu_R$  in the phenomenological calculations.

One can see that the leading twist approximation correctly describes the angular behavior for  $\pi^\pm$  production but can not describe the absolute normalization of the cross section. The comparable estimate is given only by the CZ-model in case  $\pi^+\pi^-$  production. The absolute value of the cross section obtained with the BA, BMS and set-I models is

of order of magnitude smaller than it is required by the data. The CZ-model provides much larger results because the wide DA provides the larger value of  $\langle 1/x \rangle$  and also due to the relatively low running scale used in  $\alpha_s$ . If such scenario is realized then one cannot exclude that the higher orders contributions in  $\alpha_s$  are also large. The calculation of the next-to-leading corrections can clarify this situation. Some work in this direction was already performed in Ref.[35].

But description of the  $\pi^0\pi^0$  pairs is problematic for the all models used above. It turns out that the numerically large contributions are cancel in the expressions (2.30) and (2.31). Therefore the all estimates which are based on the leading twist approach in this case provide very small values for the cross section as it is seen in Fig.2. In Ref.[11] it was suggested that the specific next-next-to-leading contributions, probably, can improve the leading order estimate.

On the other side the different phenomenological estimates such light-cone wave functions [28–30], sum rules [31, 32] and light cone sum rules [16] suggest an alternative scenario for the pion production mechanism. In this case the solution is provided by the large power corrections associated with the soft-overlap contribution. Such scenario was considered for two-pion production in the framework of the so-called handbag model in Refs.[17, 18]. In the present work are also going to study the subleading power contributions but within the systematic factorization approach. We will use the SCET framework in order to account the soft and collinear modes and to describe the soft-overlap mechanism and reduce the model dependence to a minimum.

### 3 Factorization of the subleading amplitudes in SCET

#### 3.1 Soft Collinear Effective Theory approach: general remarks

The structure of the subleading power amplitude is complicate and can be described by the different contributions associated with the different momentum regions. In what follow we assume that for the description of the relevant regions it is enough to consider the particles which have hard  $p_h$ , hard-collinear  $p_{hc}$ , collinear  $p_c$  and soft  $p_s$  momenta. The light-cone components  $(pn, p\bar{n}, p_\perp) \equiv (p_+, p_-, p_\perp)$  of the corresponding momenta scale as

$$p_h \sim Q(1, 1, 1), \quad p_h^2 \sim Q^2, \quad (3.1)$$

$$p_{hc} \sim Q(1, \lambda^2, \lambda) \text{ or } p'_{hc} \sim Q(\lambda^2, 1, \lambda), \quad p_{hc}^2 \sim Q^2\lambda^2 \sim Q\Lambda, \quad (3.2)$$

$$p_c \sim Q(1, \lambda^4, \lambda^2) \text{ or } p'_c \sim Q(\lambda^4, 1, \lambda^2), \quad p_c^2 \sim Q^2\lambda^4 \sim \Lambda^2, \quad (3.3)$$

$$p_s \sim Q(\lambda^2, \lambda^2, \lambda^2), \quad p_s^2 \sim Q^2\lambda^4 \sim \Lambda^2. \quad (3.4)$$

Here  $Q$  and  $\Lambda$  denote the generic large and soft scale, respectively. The small dimensionless parameter  $\lambda \sim \sqrt{\Lambda/Q}$ . Let us assume that there is no other the modes required for the factorization of the subleading power amplitude. In this case the factorization can be obtained in two steps: first, we integrate out the hard modes and reduce full QCD to the effective theory. Then the corresponding effective Lagrangian is constructed from the hard-collinear, collinear and soft particles. This effective theory is denoted as SCET-I. If

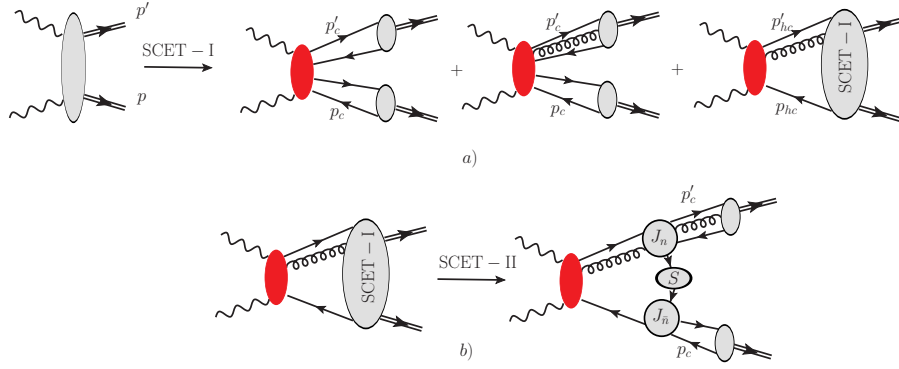


**Figure 3.** The schematical description of the SCET-I and SCET-II factorization for the process  $\gamma\gamma \rightarrow \pi\pi$  in the large angle kinematics.

the hard scale  $Q$  is so large that the hard collinear scale  $\mu_{hc} \sim \sqrt{Q\Lambda}$  is a good parameter for the perturbative expansion then one can perform the second matching step and integrate out the hard-collinear modes. Then the resulting effective Lagrangian is constructed only from the collinear and soft fields and corresponding effective theory is denoted SCET-II. Schematically this two-step factorization is illustrated in Fig.3. In Fig.3(a) we show the matching from QCD to SCET-I. The factorization of the hard particles is described by the two configurations which we will call hard (first two diagrams on the *rhs* of figure 3(a)) and soft-overlap. The hard configurations after factorization are described by the color-singlet collinear operators which overlap with the pion states due to the small invariant mass. In the leading power approximation these operators are constructed from the two collinear quark fields and have the minimal SCET dimension (or leading twist). Corresponding contribution is shown as the first diagram in Fig.3(a). The transition to SCET-II in this case can be done easily, the soft modes are decoupled and therefore can be integrated out. Such configuration describes the leading power approximation. However for subleading power corrections the soft and collinear sectors can overlap and therefore one has to consider also the subprocess with the hard-collinear modes. This situation is described schematically by the diagram with SCET-I blob in Fig.3(a). The factorization of the hard-collinear particles is shown schematically in Fig.3(b). The jet functions  $J_n$  and  $J_{\bar{n}}$  absorb the hard-collinear fluctuations (hard-collinear coefficient functions) and the soft blob  $S$  describes the subprocess with the soft particles. The collinear jets with the momenta  $p_c$  and  $p'_c$  overlap with the pion states. The second and third diagrams in Fig.3(a) describe the subleading power contributions. The gluon line in these diagrams corresponds to the transverse collinear or hard-collinear gluon.

This is a schematic picture which shows only the one possible contribution for simplicity. The realistic subleading contribution is more complicate and consist of many terms with the different structures. The SCET framework allows one to establish systematically the all of these contributions and perform an estimate of their power behavior.<sup>2</sup> Let us fix some useful notations before we start to discuss this analysis in details.

<sup>2</sup>Assuming that the all relevant configurations are described by the particles as defined in Eqs.(3.1-3.4).

The different formulation of the SCET can be found in Refs.[19–24]. In our work we use the technique developed in the position space in Refs.[23, 24]. For the SCET fields we use following notations. The fields  $\xi_n^C$ ,  $A_{\mu C}^{(n)}$  and  $\xi_{\bar{n}}^C$ ,  $A_{\mu C}^{(\bar{n})}$  denote the hard-collinear ( $C = hc$ ) or collinear ( $C = c$ ) quark and gluon fields associated with momentum  $p'$  and  $p$ , respectively, see Eq.(2.6). As usually, the hard-collinear and collinear quark fields satisfy to

$$\not{n}\xi_n^C = 0, \quad \not{n}\xi_{\bar{n}}^C = 0. \quad (3.5)$$

The fields  $q$  and  $A_\mu^{(s)}$  denote the soft quarks and gluons with the soft momenta as in Eq.(3.4) which also enter in the SCET Lagrangian. We will use the convenient notation for the gauge invariant combinations often appearing in SCET such as

$$\chi_n^C(\lambda\bar{n}) \equiv W_n^\dagger(\lambda\bar{n})\xi_n^C(\lambda\bar{n}), \quad \bar{\chi}_n^C(\lambda\bar{n}) \equiv \bar{\xi}_n^C(\lambda\bar{n})W_n(\lambda\bar{n}), \quad (3.6)$$

$$A_{\mu C}^{(n)}(\lambda\bar{n}) \equiv \left[ W_n^\dagger(\lambda\bar{n})D_{\mu C}W_n(\lambda\bar{n}) \right], \quad (3.7)$$

where the covariant derivative  $D_{\mu C} = i\partial_\mu + gA_{\mu C}^{(n)}$  acts inside the brackets and the hard-collinear or collinear gluon Wilson line (WL) read:

$$W_n(z) = \text{P exp} \left\{ ig \int_{-\infty}^0 ds \, \bar{n} \cdot A_C^{(n)}(z + s\bar{n}) \right\}. \quad (3.8)$$

In the wide-angle kinematics we have the energetic particles propagating with large energies in four directions. Therefore it is useful to introduce two more auxiliary light-cone vectors associated with the photon momenta:  $q_1$  and  $q_2$

$$\bar{v}^\mu = \frac{2q_1^\mu}{\sqrt{s}}, \quad v^\mu = \frac{2q_2^\mu}{\sqrt{s}}, \quad (\bar{v} \cdot v) = 2. \quad (3.9)$$

Using the vectors  $\bar{v}, v$  we also introduce the hard-collinear quark and gluon fields in the similar way as before just changing  $(n, \bar{n}) \rightarrow (v, \bar{v})$ .

The explicit expression for the SCET-I Lagrangian in position space can be found in Refs.[23, 24]. This Lagrangian being expanded in the small parameter  $\lambda$  is given by the sum

$$\mathcal{L}_{\text{SCET}}^{(n)} = \mathcal{L}_{\xi\xi}^{(n,0)} + \mathcal{L}_{\xi\xi}^{(n,1)} + \mathcal{L}_{q\xi}^{(n,1)} + \mathcal{O}(\lambda^2), \quad (3.10)$$

where  $\mathcal{L}_{\xi\xi}^{(n,\lambda)} \sim \mathcal{O}(\lambda)$  and the explicit expressions read

$$\mathcal{L}_{\xi\xi}^{(n,0)} = \bar{\xi}_n^C(x) \left( i n \cdot D + g n \cdot A^{(s)}(x_-) + i \not{D}_\perp \frac{1}{i\bar{n} \cdot D} i \not{D}_\perp \right) \frac{\not{n}}{2} \xi_n^C(x), \quad (3.11)$$

$$\mathcal{L}_{q\xi}^{(n,1)} = \bar{\xi}_n^C(x) i \not{D}_\perp W_n q(x_-) + \bar{q}(x_-) W_n^\dagger i \not{D}_\perp \xi_n^C(x). \quad (3.12)$$

where  $D_\mu = i\partial_\mu + gA_{\mu C}^{(n)}$ ,  $x_- = \frac{1}{2}(x\bar{n})n$ . The expression for the subleading term  $\mathcal{L}_{\xi\xi}^{(n,1)}$  is a bit lengthy and we will not write it here. The similar expressions are also valid for the other collinear sectors associated with the directions  $\bar{n}, v, \bar{v}$ .

Performing the matching from SCET-I to SCET-II one substitutes  $\xi_n^C \rightarrow \xi_n^c + \xi_n^{hc}$  and  $A_C^{(n)} \rightarrow A_c^{(n)} + A_{hc}^{(n)}$  in (3.10) and integrate out hard-collinear fields. A more detailed

description of this step can be found in Refs.[36, 37] in the hybrid representation and in Ref.[38] in the position space formulation. In our work we will consider mainly the first matching step for the soft-overlap contributions and SCET-II factorization for the hard rescattering terms.

The power counting rules for different SCET operators can be fixed using the power counting of the SCET fields. The counting rules for the SCET fields can be obtained from the corresponding propagators in momentum space and read (see for instance Ref.[23])

$$\xi_n^{hc} \sim \lambda, \quad \bar{n} \cdot A_{hc}^{(n)} \sim 1, \quad A_{\perp hc}^{(n)} \sim \lambda, \quad n \cdot A_{hc}^{(n)} \sim \lambda^2, \quad (3.13)$$

$$\xi_n^c \sim \lambda^2, \quad \bar{n} \cdot A_c^{(n)} \sim 1, \quad A_{\perp c}^{(n)} \sim \lambda^2, \quad n \cdot A_c^{(n)} \sim \lambda^4, \quad (3.14)$$

$$A_s^\mu \sim \lambda^2, \quad q \sim \lambda^3. \quad (3.15)$$

In order to find the scaling behavior of the amplitudes one has to consider the matrix elements of the SCET operators. Therefore we need also to define the power counting for external hadronic states. In our frame the outgoing pions are made of energetic collinear partons therefore assuming the conventional normalization of hadronic states one obtains

$$\langle \pi(p_c) | \sim \lambda^{-2}. \quad (3.16)$$

Using this counting one obtains easily the scaling behavior of the leading twist pion DA defined in Eq.(2.23)

$$\langle \pi(p') | \bar{\chi}_n^c(\lambda \bar{n}) \not{n} \gamma_5 \chi_n^c(0) | 0 \rangle \sim Q^2 \lambda^2 \sim Q \Lambda. \quad (3.17)$$

In the analysis carried out below we will also need the higher twist pion distribution amplitudes. Because the invariant mass of the each produced pions is restricted to order  $Q^2 \lambda^4 \sim \Lambda^2$  only the pure collinear operator in SCET can be matched onto the hadronic states. Schematically the full set of the required collinear operators  $O_n^{(i)} \sim \mathcal{O}(\lambda^i)$  up to twist-4 is given by the following three subsets

$$O_n^{(4)} = \bar{\chi}_n^c \not{n} \gamma_5 \chi_n^c, \quad (3.18)$$

$$O_n^{(6)} = \bar{\chi}_n^c \not{n} \gamma_\perp^\mu \gamma_5 \mathcal{A}_{\mu\perp}^{(n)} \chi_n^c, \quad (3.19)$$

$$O_n^{(8)} = \left\{ \bar{\chi}_n^c \Gamma \gamma_5 \mathcal{A}_{\mu\perp}^{(n)} \mathcal{A}_{\nu\perp}^{(n)} \chi_n^c, \bar{\chi}_n^c \not{n} \gamma_5 (n \cdot \mathcal{A}^{(n)}) \chi_n^c, \right. \\ \left. \bar{\chi}_n^c \not{n} i \varepsilon_\perp^{\mu\nu} \left[ D_{\nu\perp} \mathcal{A}_{\mu\perp}^{(n)} \right] \chi_n^c, \bar{\chi}_n^c \Gamma_1 \chi_n^c \bar{\chi}_n^c \Gamma_2 \chi_n^c \right\}. \quad (3.20)$$

All these operators are color singlet, for simplicity we also do not show their flavor structure. The matrix  $\Gamma$  denotes the appropriate Lorentz structure for the each particular case. The qualitative description given in Eqs.(3.18-3.20) is enough for our purpose. The similar set of the collinear operators also exists in the  $\bar{n}$ -collinear sector. More detailed description of the higher twist collinear operators in the hybrid SCET formulation can be also found in Ref.[39]. For convenience, in Appendix A we provide the QCD definitions of the higher twist DAs for pion up to twist four.

Real photon has also nonperturbative component of the wave function and therefore one can define the matrix element which defines the photon DA. The leading twist DA is defined by the chiral-odd operator Ref.[40]

$$O_v^{(4)} = \bar{\chi}_v^c \not{n} \gamma_\perp \chi_v^c \quad (3.21)$$

where we assume that the basic light-like vectors are  $v$  and  $\bar{n}$  and  $\gamma_\perp$  denotes the transverse projection with respect to these basis. The choice of the second light-like vector in Eq.(3.21) is not relevant now and we will not discuss it.

### 3.2 Analysis of the subleading power contributions in SCET

In the framework of the SCET approach the subleading power corrections are described by the subleading operators constructed from the fields in SCET-I. In order to perform a systematic analysis of the subleading power contributions we have to consider all possible subleading operators which can be relevant to a given accuracy.

The factorization of the hard modes can be described as a matching of the T-product of the electromagnetic currents onto SCET-I operators. The result can be written as

$$\begin{aligned} T \{ J_{\text{em}}^\mu, J_{\text{em}}^\nu \} &= \sum_i H_i^{\mu\nu} * O^{(i)} + \sum_i C_{\gamma i}^\mu * T \{ O_\gamma^{(i)}, J_{\text{em}}^\nu \} \\ &+ \sum_i C_{\gamma\gamma}^{(i)} * T \{ O_{\gamma\gamma}^{(i)}, J_{\text{em}}^\mu, J_{\text{em}}^\nu \}. \end{aligned} \quad (3.22)$$

The three contributions in Eq.(3.22) correspond the three general configurations associated with the different hard subprocesses. The first term describes the configuration where both point-like photons participate in the hard scattering and couple to the hard quarks. The second and the third terms in Eq.(3.22) describe the configurations where one or both photons are nonperturbative and must be considered as a hadronic state. These configurations can appear only as subleading power contributions because we will show that the operators  $O_\gamma^{(i)}$  and  $O_{\gamma\gamma}^{(i)}$  are subleading according to the SCET counting rules comparing to the operators  $O^{(i)}$  in the first term.

In the subsequent analysis we will distinguish two different cases associated with the two different groups of the operators. Assume that the operators  $O^{(i)}$ ,  $O_\gamma^{(i)}$  or  $O_{\gamma\gamma}^{(i)}$  are constructed only from the collinear fields which can describe overlap with the *in/out* collinear hadronic states. We will call such contributions “hard” in order to stress the absence of the hard-collinear and soft subprocesses. All other operators which are built from the combination of the hard-collinear, collinear and soft fields can be associated with the soft-overlap contribution. Hence we will call corresponding matrix elements as “soft-overlap” or simply soft. Following this classification and taking into account definition (2.22) we rewrite the subleading contribution as a sum of hard and soft contributions

$$B_{+\pm}^{(i)} = B_{+\pm}^{(i,h)} + B_{+\pm}^{(i,s)}. \quad (3.23)$$

However the overlap of the collinear and soft sectors leads to a mixing of the hard and soft configurations and to appearing of the large rapidity logarithms. This effect is related with the so-called end-point singularities in the hard contributions. Therefore the definition

of the hard and soft parts in Eq.(3.23) is rather formal because it must be completed by rapidity regularization. In the present paper we will follow to a different approach and therefore we will use the formal definition as explained above.

As a starting point let us discuss the hard contributions. Consider the first term in Eq.(3.22). Here  $H^{\mu\nu}$  denotes the hard coefficient function and the operators  $O^{(i)}$  must be constructed from the collinear fields. The simplest relevant hard configuration which can be constructed from the collinear fields is described by the four quark operator and reads

$$O_c^{(8)} = O_n^{(4)} O_{\bar{n}}^{(4)} = (\bar{\chi}_n^c \not{n} \gamma_5 \chi_n^c) (\bar{\chi}_{\bar{n}}^c \not{\bar{n}} \gamma_5 \chi_{\bar{n}}^c), \quad (3.24)$$

where the operators  $O_{n,\bar{n}}^{(4)}$  defined in Eq.(3.18). Each of these operators is of order  $\lambda^4$ . The absence of the hard-collinear fields allows one to pass to the SCET-II. Because of decoupling of the soft and collinear modes at leading power in SCET-II Lagrangian [36, 38] the matrix element of the collinear operators factorizes

$$\langle p, p' | O_n^{(4)} O_{\bar{n}}^{(4)} | 0 \rangle_{\text{SCETII}} = \langle p | O_n^{(4)} | 0 \rangle_{\text{SCETII}} \langle p' | O_{\bar{n}}^{(4)} | 0 \rangle_{\text{SCETII}}. \quad (3.25)$$

It is easy to understand that in QCD it is not possible to construct the collinear operator  $O_n^{(\lambda)}$  with  $\lambda < 4$  which has nontrivial matrix element, i.e.

$$\langle \pi(p) | O_n^{(\lambda)} | 0 \rangle_{\text{SCETII}} = 0, \quad \lambda < 4. \quad (3.26)$$

This observation explains why we obtain the first nontrivial operator only at order  $\lambda^8$ . Substituting parametrization of the matrix elements (2.23) and performing Fourier transformation we obtain the factorization formulas discussed in Sec.2.2. The scaling behavior of this contribution can be easily obtained using the SCET counting rules that gives

$$A_{+\pm}^{(i)} \sim \underbrace{\langle p' | O_n^{(4)} | 0 \rangle_{\text{SCETII}}}_{\lambda^2} * H^{\mu\nu} * \underbrace{\langle p | O_{\bar{n}}^{(4)} | 0 \rangle_{\text{SCETII}}}_{\lambda^2} \sim \lambda^4 \sim \Lambda^2/Q^2. \quad (3.27)$$

This is in agreement with the results presented in Sec.2.2. In order to prove the leading power factorization formula within the SCET framework one must show that the soft-overlap contributions can not provide the same collinear operator  $O_c^{(8)}$  with the same scaling behavior after integration over hard-collinear modes. If this property is fulfilled then the leading order factorization discussed in Sec.2.2 is established. Below we prove the leading twist factorization performing the analysis of the soft subleading contributions.

Let us now consider the subleading collinear operators which are relevant for the hard contribution  $B_{+\pm}^{(i,h)}$ . Combining the collinear operators listed in Eqs.(3.18-3.20) and (3.21) we construct the operators up to order  $\lambda^{12}$ . They have following structure

$$O_c^{(10)} = O_n^{(6)} O_{\bar{n}}^{(4)} + O_n^{(4)} O_{\bar{n}}^{(6)}, \quad (3.28)$$

$$O_{\gamma c}^{(12)} = O_n^{(4)} O_{\bar{n}}^{(4)} O_v^{(4)}, \quad O_n^{(4)} O_{\bar{n}}^{(4)} O_{\bar{v}}^{(4)}, \quad (3.29)$$

$$O_c^{(12)} = O_n^{(6)} O_{\bar{n}}^{(6)}, \quad O_n^{(4)} O_{\bar{n}}^{(8)} + O_n^{(8)} O_{\bar{n}}^{(4)}, \quad (3.30)$$

where  $O_n^{(8)}$  denotes the arbitrary collinear operators from the set in Eq.(3.20). The operator  $O_c^{(10)}$  scales as  $\lambda^{10}$  but the operator  $O_n^{(6)}$  is chiral odd and  $O_{\bar{n}}^{(4)}$  is chiral even. Therefore



corresponding hard coefficient function vanishes for massless quarks and this operator can be neglected. The same arguments are applicable also for the operator  $O_{\gamma_c}^{(12)}$  which describe the contribution with the one nonperturbative photon. The photon operator  $O_v^{(4)}$  is chiral odd, see Eq.(3.21). Therefore we are left only with the operators defined in Eq.(3.30). All these operators scales as  $\lambda^{12}$  and therefore define the contributions which give  $\mathcal{O}(\lambda^4)$  corrections to the leading power approximation.

Computing these contributions one finds that collinear convolution integrals are singular at the end-point region. Below we demonstrate this explicitly computing the contribution associated with the  $O_n^{(6)} O_{\bar{n}}^{(6)}$  operator. These singularities indicate the overlap between the soft and collinear regions that leads to the overlap between the hard and soft-overlap contributions. Therefore in order to be consistent one must also include the appropriate soft-overlap contributions.

The soft-overlap contribution is described by operators with the hard-collinear fields. We also divide these operators on three groups according to structure in Eq.(3.22). The first group is related with the operator  $O^{(i)}$  and consist of the fields associated only with the  $n$  and  $\bar{n}$  hard-collinear sectors. Therefore these operators describe the soft-collinear overlap between the produced pions. In Fig.3(a) the contribution of such an operator is shown by third diagram on *rhs*. Taking into account  $C$ -parity of the two-pion state one can easily construct the set of the relevant operators. More explicitly we must consider all SCET-I operators which can provide after matching to SCET-II the operator of order  $\lambda^{12}$ . In addition the resulting SCET-II operator must have the following structure

$$O_n^{(\lambda)} O_{\bar{n}}^{(\lambda)} [q\bar{q} \dots] \quad (3.31)$$

in order to match the pion states. The dots in the brackets denote additional soft quark-antiquark or gluon fields. Below we list the suitable SCET-I operators up to order  $\lambda^6$ . They read

$$O_g^{(2)} = A_{\perp\mu}^{(n)} A_{\perp\nu}^{(\bar{n})}, \quad (3.32)$$

$$O^{(3)} = \bar{\chi}_n \left( \mathcal{A}_{\perp}^{(n)} + \mathcal{A}_{\perp}^{(\bar{n})} \right) \chi_{\bar{n}} + (n \leftrightarrow \bar{n}), \quad (3.33)$$

$$O_3^{(4)} = \left\{ \bar{\chi}_n \left( \mathcal{A}_{\perp c}^{(n)} + \mathcal{A}_{\perp c}^{(\bar{n})} \right) \chi_{\bar{n}} + (n \leftrightarrow \bar{n}), \bar{\chi}_{n\perp}^c \mathcal{A}_{\perp}^{(n)} \chi_{\bar{n}} + (n \leftrightarrow \bar{n}), \bar{\chi}_n \mathcal{A}_{\perp}^{(\bar{n})} \chi_{\bar{n}}^c + (n \leftrightarrow \bar{n}) \right\} \quad (3.34)$$

$$O_4^{(5)} = \left\{ \bar{\chi}_n \mathcal{A}_{\perp}^{(n)} \left( n \cdot \mathcal{A}_{\perp}^{(n)} \right) \chi_{\bar{n}} + (n \leftrightarrow \bar{n}), \bar{\chi}_n \mathcal{A}_{\perp}^{(n)} \left( \bar{n} \cdot \mathcal{A}_{\perp}^{(\bar{n})} \right) \chi_{\bar{n}} + (n \leftrightarrow \bar{n}), \right. \quad (3.35)$$

$$\left. \bar{\chi}_n \mathcal{A}_{\perp}^{(\bar{n})} \left( \bar{n} \cdot \mathcal{A}_{\perp}^{(\bar{n})} \right) \chi_{\bar{n}} + (n \leftrightarrow \bar{n}), \bar{\chi}_n \mathcal{A}_{\perp}^{(\bar{n})} \left( n \cdot \mathcal{A}_{\perp}^{(n)} \right) \chi_{\bar{n}} + (n \leftrightarrow \bar{n}) \right\}, \quad (3.36)$$

$$O^{(5)} = \left\{ \bar{\chi}_n \mathcal{A}_{\perp}^{(n)} \mathcal{A}_{\perp\mu}^{(n)} \mathcal{A}_{\perp\nu}^{(n)} \chi_{\bar{n}} + (n \leftrightarrow \bar{n}), \bar{\chi}_n \mathcal{A}_{\perp}^{(n)} \mathcal{A}_{\perp\mu}^{(n)} \mathcal{A}_{\perp\nu}^{(\bar{n})} \chi_{\bar{n}} + (n \leftrightarrow \bar{n}), \dots \right\}. \quad (3.37)$$

Here and further we do not show the hard-collinear indices of the fields and assume, for simplicity

$$\bar{\chi}_n \equiv \bar{\chi}_n^{hc}, \mathcal{A}_{\perp}^{(n)} \equiv \mathcal{A}_{\perp hc}^{(n)}. \quad (3.38)$$

The collinear fields are always shown with the subscript  $c$ . The dots in Eq.(3.37) denotes the similar operators with the three transverse hard-collinear gluon fields but with the

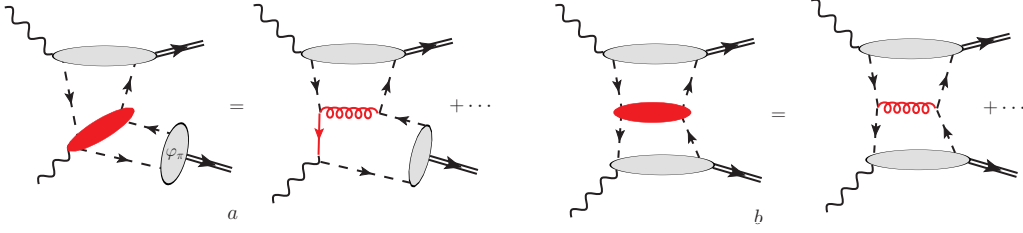


**Figure 4.** Examples of the different configurations associated with the operators  $O_\gamma^{(i)}$  (a) and  $O_{\gamma\gamma}^{(i)}$  (b). The red blob and lines show the hard subprocess. The dashed quark lines describe the hard-collinear particles, the gray blobs describe the hard-collinear, collinear and soft subprocesses.

different combinations of collinear indices ( $n$ ) and ( $\bar{n}$ ). There are also relevant operators of order  $\lambda^6$  and higher but we will not consider them for reasons explained later.

In the given list of the SCET-I operators we excluded the operators with odd number of transverse indices and with the chiral odd structures like

$$\bar{\chi}_n \gamma_\perp^\rho \chi_{\bar{n}}, \quad \bar{\chi}_n \mathcal{A}_\perp^{(n)} \mathcal{A}_{\perp\mu}^{(n)} \chi_{\bar{n}}, \quad \bar{\chi}_n \mathcal{A}_\perp^{(n)} \mathcal{A}_{\perp\mu}^{(n)} \chi_{\bar{n}}, \quad \bar{\chi}_n \gamma_\perp^\sigma \gamma_\perp^\rho \chi_{\bar{n}}, \quad (3.39)$$

and so on. The two-pion SCET-I matrix element from the operators with odd number of transverse indices are trivial because of Lorentz symmetry. For instance

$$\langle p', p | \bar{\chi}_n \gamma_\perp^\rho \chi_{\bar{n}} | 0 \rangle_{\text{SCET-I}} = 0, \quad (3.40)$$

because one does not have any transverse vector in order to describe the transverse structure of the quark operator. The operators with the chiral-odd structure were neglected because they can not arise from the perturbative diagrams with the massless particles.

The operators  $O_\gamma^{(i)}$  and  $O_{\gamma\gamma}^{(i)}$  in Eq.(3.22) can be associated with the diagrams shown in Fig.4. Corresponding configurations describe the soft-overlap of the photon with the hadronic state. These are four-fermion operators, for instance (for simplicity we do not show the color and flavor structure)

$$O_\gamma^{(6)} = \bar{\chi}_v \Gamma \chi_n O_{\bar{n}}^{(4)}, \quad \dots, \quad (3.41)$$

$$O_{\gamma\gamma}^{(4)} = \bar{\chi}_v \Gamma \chi_{\bar{v}} \bar{\chi}_n \Gamma \chi_{\bar{n}}, \quad \dots \quad (3.42)$$

Here the symbol  $\Gamma$  again denotes a suitable Lorentz structure, dots denote the other possible combinations with the similar SCET structure. The operators in Eqs.(3.41) and (3.42) have the minimal SCET dimension among the operators which can describe the required soft-overlap configuration.

If the hard-collinear scale is not large enough then one can not perform the further matching on SCET-II. We suppose that this situation is actual for the phenomenological analysis of the existing data. Therefore we consider the SCET-I matrix elements as unknown nonperturbative quantities. Then the expected factorization formula reads as a following sum of the different contributions

$$B_{+\pm}^{(i)} = \sum C_{+\pm}^{(i,s)} * f_{\pi\pi} + \sum \varphi * C_{\gamma+\pm}^{(i,s)} * f_{\gamma\pi}^{(2)} + \sum C_{\gamma\gamma+\pm}^{(i,s)} * f_{\gamma\pi}^{(4)} + \sum \varphi * H_{+\pm}^{(i,h)} * \varphi. \quad (3.43)$$

These result includes of the soft and hard terms. The SCET amplitudes  $f_{\pi\pi}$ ,  $f_{\gamma\pi}^{(2)}$  and  $f_{\gamma\pi}^{(4)}$  denote the contributions of the SCET-I matrix elements of the operators  $O^{(\lambda)}$ ,  $O_{\gamma}^{(\lambda)}$  and  $O_{\gamma\gamma}^{(\lambda)}$ , respectively. The symbol  $\varphi$  in Eq.(3.43) denotes the all possible leading and subleading twist DAs which can appear in the hard term. SCET-I matrix elements and DAs are unknown nonperturbative matrix elements, the sums in Eq.(3.43) denote schematically the summation over the all relevant independent operators discussed above.

From the previous consideration it follows that we obtain many SCET-I unknown amplitudes and therefore the general consideration of the power subleading factorization becomes very complicate. In order to simplify our analysis we reduce now our consideration only to the leading-order or leading-logarithmic accuracy. This means that we consider only such contributions which can appear at leading-order in hard QCD coupling  $\alpha_s(Q^2)$ , where  $Q$  denotes a generic hard scale. The hard coefficient functions  $H_{+\pm}^{(i,h)}$  in Eq.(3.43) describe in the hard contributions  $B_{+\pm}^{(i,h)}$  and have the leading order contributions of order  $\alpha_s$  because they arise from the matching onto collinear four-quark operators. These hard contributions mix with the appropriate soft contributions due to the overlap of the soft and collinear sectors. The relevant hard coefficient functions  $C_{+\pm}^{(i,s)}$  in Eq.(3.43) describing the two-pion soft-overlap configuration arise already at Born level  $\sim \alpha_s^0$ . Hence we can exclude from our analysis the SCET-I operators with the subleading in hard  $\alpha_s$  coefficient functions. In particular, this allows us to neglect the discussion of the configurations associated with  $O_{\gamma}^{(i)}$  and  $O_{\gamma\gamma}^{(i)}$  because the corresponding hard coefficient functions are of order  $\alpha_s$ , see Fig.4. Then we are left only with the contributions from the operators  $O^{(\lambda)}$  which describe the soft-collinear overlap of the two-pion state. The specific feature of these contributions is that SCET-I matrix elements depend only from  $s$

$$\langle p, p' | O^{(\lambda)} | 0 \rangle_{\text{SCET-I}} \sim f_{\pi\pi}(s). \quad (3.44)$$

Let us remind, that this  $s$ -dependence is associated with the hard-collinear subprocess because we already factorized the hard particles which have virtualities of order  $1/s$ . Farther we will call the unknown functions  $f_{\pi\pi}(s)$  as SCET form factors (FFs).

In what follow we assume that at the leading-order accuracy the factorization formula (3.43) simplifies and can be described by the sum only of two contributions

$$B_{+\pm}^{(i)}(s, \theta) \simeq \sum C_{+\pm}^{(i,s)}(s, \theta) * f_{\pi\pi}(s) + \sum \varphi * H_{+\pm}^{(i,h)}(s, \theta) * \varphi. \quad (3.45)$$

Here the hard coefficient functions  $C_{+\pm}^{(i,s)}$  and  $H_{+\pm}^{(i,h)}$  are of order  $\mathcal{O}(1)$  and  $\mathcal{O}(\alpha_s)$ , respectively. The hard configuration is described by the matrix elements from the collinear operators (3.30), the asterisks denote the collinear convolution integrals. The soft part is described by the SCET-I operators listed in Eqs.(3.32-3.37). The sums denote schematically the summation over the all relevant operators which describe the matrix elements in the hard and soft contributions.

The hard and soft terms in Eq.(3.45) are not well defined separately due to the overlap between the collinear and soft regions as we already discussed. As a result one observes usually the end-point singularities in the collinear convolution integrals. In the soft term the end-point singularities become evident only after the matching on SCET-II where the

factorization is described in terms of the soft and collinear functions. Therefore one has to assume a suitable regularization in the Eq.(3.45). Such regularization introduces the explicit dependence on the regularization scheme and appears to be very inconvenient for the phenomenological analysis. This problem can be resolved if it is possible to formulate the framework which allows one to resum the large rapidity logarithms to all orders. However at present time such approach is still challenging. Nevertheless in a certain situation one can reformulate the factorization formula and to exclude the end-point singularities. It turns out that this method can also be applied in our case therefore let us discuss it in detail.

One can see from Eq.(3.45) that the dependence on the scattering angle  $\theta$  is completely defined by the hard rescattering because it appears only in the hard coefficient functions. This observation allows one to solve the problem with the end-point singularities in the hard contribution using the idea of the physical subtraction scheme [41, 42]. Consider for simplicity a situation with one SCET-I form factor and assume that the factorization formula can be written as

$$B(s, \theta) \simeq C(s, \theta) f_{\pi\pi}(s) + \varphi * H(s, \theta) * \varphi, \quad (3.46)$$

where we simplified notation assuming

$$B(s, \theta) \equiv B_{+\pm}^{(i)}(s, \theta), \quad C(s, \theta) \equiv C_{+\pm}^{(i,s)}(s, \theta), \quad H(s, \theta) \equiv H_{+\pm}^{(i,h)}(s, \theta). \quad (3.47)$$

In Eq.(3.46) we make the important assumption which is related to the structure of the soft-overlap contribution. We assume that the hard coefficient function  $C(s, \theta)$  enters as a simple multiplicative factor in front of SCET FF  $f_{\pi\pi}(s)$ . In certain cases this assumption is realized very easily. For instance, if the SCET-I operator describing  $f_{\pi\pi}(s)$  consist of two SCET fields associated with the different collinear sectors. However if the operator has two or more hard-collinear fields associated with the same sector then the soft term in factorization formula is given by the convolution integral over collinear fractions and structure assumed in Eq.(3.46) is not obvious anymore. Let us postpone the discussion of this point for a future and assume that ( ° fBfact) is also valid in our case.

Then using Eq.(3.46) one can express the unknown SCET FF  $f_{\pi\pi}(s)$  through the physical amplitude  $B(s, \theta_0)$  at some fixed angle  $\theta_0$

$$f_{\pi\pi}(s) = \frac{B(s, \theta_0)}{C(s, \theta_0)} - \varphi * \frac{H(s, \theta_0)}{C(s, \theta_0)} * \varphi. \quad (3.48)$$

The choice of the  $\theta_0$  is not fixed except the applicability of the expression (3.46) at this value of  $\theta$ . Then substituting this value of  $f_{\pi\pi}$  for the general expression we obtain

$$B(s, \theta) \simeq \frac{C(s, \theta)}{C(s, \theta_0)} B(s, \theta_0) + \varphi * \left[ H(s, \theta) - \frac{C(s, \theta)}{C(s, \theta_0)} H(s, \theta_0) \right] * \varphi. \quad (3.49)$$

Now the expression for the hard scattering term  $\varphi_\pi * [\dots] * \varphi_\pi$  must be well defined because all other terms in Eq.(3.49) are free from the any singularities. This means that the singular in the end-point region contributions cancel in the difference describing the hard term in

Eq.(Bphys). Such approach is very convenient because it allows one to fix the unknown FF  $f_{\pi\pi}$  in terms of physical quantity and to obtain the well defined expression for the amplitude. The value  $B(s, \theta_0)$  in many cases can be fixed from the experimental data. In this case using Eq.(3.49) for analysis of the data allows one to verify the  $\theta$ -dependence in a model independent way. If the expression (3.46) is valid but one has few unknown FF's  $f_{\pi\pi}^{(i)}$  then one can proceed in the same way but now one has to use few different points  $\theta_0^{(i)}$  in order to re-express all SCET FF's in terms of physical amplitudes.

In what follow we perform the analysis of the SCET-I operators  $O^{(\lambda)}$  listed in Eq.(3.32-3.34) and demonstrate that they can provide contributions which mix in SCET-II with the collinear operators in (3.30). Therefore we demonstrate that such mixing is responsible for the the soft-collinear overlap between the hard and soft contributions. After that we proceed further and compute the compute the hard coefficient functions in order to establish the applicability of the physical subtraction scheme described above.

The gluon operator in Eq.(3.32) has nonzero matrix element but the corresponding coefficient function is of order  $\alpha_s$ . Hence we neglect it as subleading contribution. Then at leading order we do not have any contribution associated with leading two-jet operators.

Consider the operators in Eqs.(3.33) and (3.34). Our aim is to estimate the scaling behavior of these operators after matching to SCET-II and to establish the structure of the resulting collinear operator. In order to see the soft-collinear overlap between the soft and hard terms the obtained SCET-II operator must have the same collinear structure and provide the same scaling behavior as the collinear operator in the hard terms. The required structure of such SCET-II operators was given in Eq.(3.31). The presence of the soft fields in Eq.(3.31) increases the power of  $\lambda$  for the such contribution but the SCET-II is not a local theory therefore the contribution of the soft sector can be compensated by the negative powers of  $\lambda$  from the contractions of the hard-collinear fields.

From the technical point of view we must consider the matching from SCET-I to SCET-II and estimate the behavior of the suitable time-ordered products in SCET-II. Consider the following time-ordered products describing the matching of the operators (3.33) and (3.34)

$$\mathcal{A} = T \left\{ O^{(3)}, \mathcal{L}_{\xi\xi}^{(n,0)}, \mathcal{L}_{q\xi}^{(n,1)}, \mathcal{L}_{\xi\xi}^{(n,0)}, \mathcal{L}_{q\xi}^{(\bar{n},1)} \right\}, \quad (3.50)$$

$$\mathcal{B} = T \left\{ O_3^{(4)}, \mathcal{L}_{\xi\xi}^{(n,0)}, \mathcal{L}_{q\xi}^{(n,1)}, \mathcal{L}_{q\xi}^{(\bar{n},1)} \right\}, \quad (3.51)$$

$$\mathcal{C} = T \left\{ O_3^{(4)}, \mathcal{L}_{\xi\xi}^{(n,0)}, \mathcal{L}_{q\xi}^{(n,1)}, \mathcal{L}_{q\xi}^{(\bar{n},2)} \right\}, \quad (3.52)$$

$$\mathcal{D} = T \left\{ O_3^{(4)}, \mathcal{L}_{\xi\xi}^{(n,0)}, \mathcal{L}_{q\xi}^{(n,2)}, \mathcal{L}_{q\xi}^{(\bar{n},1)} \right\}. \quad (3.53)$$

where  $\mathcal{L}_{\xi\xi}^{(n,0)}$  and  $\mathcal{L}_{q\xi}^{(n,1)}$  denote the leading and the subleading SCET-I Lagrangians described in Eqs.(3.11) and (3.12). The contributions with the interaction vertices generated from  $\mathcal{L}_{q\xi}^{(n,2)}$  and  $\mathcal{L}_{q\xi}^{(\bar{n},2)}$  will be clarified below. Contracting the all hard-collinear fields in the expressions described by the T-products one obtains the SCET-II operator which consist only from the collinear and soft fields. The Feynman diagrams which arise after the

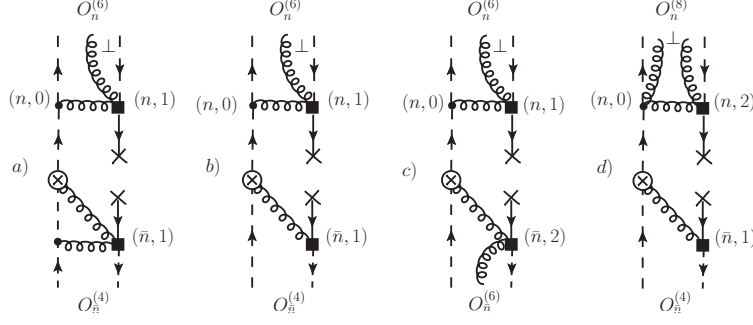


**Figure 5.** Examples of the diagrams which describe the time-ordered products  $\mathcal{A} - \mathcal{C}$  defined in Eqs. (3.50)-(3.52). Here the crossed circles describe the vertices of the SCET-I operators, dashed lines describe the hard-collinear and collinear quarks, curly line corresponds to the hard-collinear and collinear gluons. All external particles are assumed to be collinear or soft. The soft quark fields are shown by the solid lines with crosses at the ends. The black circle or square denotes the insertion of the leading and subleading vertex generated by  $\mathcal{L}_{\xi\xi}^{(0)}$  or  $\mathcal{L}_{q\xi}^{(i)}$ , respectively.

contractions of the hard-collinear fields describe the analytical expressions for the hard-collinear jet functions. The example of such diagrams are shown in Fig.5(a) – (d) for the each T-product defined in Eqs.(3.50)-(3.53), respectively. We do not specify the operator  $O_3^{(4)}$  which defines the expression for the vertex assuming that it is clear from the given example. For the each diagram in Fig.5 we indicate the expected collinear operator  $O_{n,\bar{n}}^{(\lambda)}$  in the each collinear sector. We will also see that it is important to understand the Dirac structure of the diagrams in order to pick up the nontrivial contributions. We will discuss this issue in detail below.

From the structure of diagrams in Fig.5 one can conclude that the T-products can be represented as

$$T \left\{ O^{(\lambda)}, \dots \right\} = O_n^{(\lambda')} * J_n * q\bar{q} * J_{\bar{n}} * O_{\bar{n}}^{(\lambda)} \quad (3.54)$$

where we introduced the jet-functions  $J_n$  and  $J_{\bar{n}}$ . In order to estimate scaling of each T-product one has to estimate the scaling behavior of these jet functions. This can be easily done using the given diagrams in Fig.5 and taking into account that contractions of the hard-collinear fields yield

$$\int d^4x_1 \left\langle A_{hc\perp}^\alpha(x_1) A_{hc\perp}^\beta(x_2) \right\rangle \sim \int d^4x_2 \left\langle (\bar{n} \cdot A_{hc})(x_2) (n \cdot A_{hc})(x_3) \right\rangle \sim \lambda^{-2}, \quad (3.55)$$

$$\int d^4x_3 \left\langle \bar{\xi}_{hc}(x_1) \xi_{hc}(x_3) \right\rangle \sim \lambda^{-2}, \quad (3.56)$$

i.e. all hard-collinear contractions provide  $\lambda^{-2}$  which results from the hard-collinear propagators in momentum space.

Then for the first two diagrams describing T-products  $\mathcal{A}$  and  $\mathcal{B}$  we obtain

$$\mathcal{A} \sim \mathcal{B} \sim O_n^{(6)} * J_n * q\bar{q} * J_{\bar{n}} * O_{\bar{n}}^{(4)} \sim \lambda^6 \times \lambda^{-4} \times (\lambda^3)^2 \times \lambda^{-2} \times \lambda^4 \sim \lambda^{10}. \quad (3.57)$$

Both T-products provide the same SCET-II operator and have the same scaling behavior. The operator  $O^{(3)}$  differs from the operators  $O^{(43)}$  only by one hard-collinear field. As a

result it requires the additional hard-collinear contraction appearing of the hard-collinear loop for  $J_{\bar{n}}$  in the T-product  $\mathcal{A}$ . This loop have the three propagators which together with integral measure yield the estimate  $\lambda^{-2}$ , i.e. the same as simple hard-collinear propagator in the digram in Fig.5(b). One can conclude that these operators describe the same SCET-II output but at the different orders in the SCET-I perturbation expansion.

An interesting observation is that these contributions are less suppressed then it is expected from the behavior of the hard configuration which is of order  $\lambda^{12}$ . Such result is closely related to the fact that corresponding collinear operators in Eq.(3.57) have different chirality:  $O_n^{(6)}$  is chiral-odd and  $O_{\bar{n}}^{(4)}$  is chiral-even. Earlier we already discussed that such configuration can not appear in the hard contribution because of massless quarks in the diagrams describing a hard subprocess. But in the soft-overlap contribution the quark line is soft and described by the light-cone correlator<sup>3</sup>

$$\hat{S}_{\alpha\beta} = \langle 0 | q_\alpha(\lambda\bar{n})\bar{q}_\beta(\eta n) | 0 \rangle = S_n[\not{n}]_{\alpha\beta} + S_{\bar{n}}[\not{\bar{n}}]_{\alpha\beta} + S_m[I]_{\alpha\beta}, \quad (3.58)$$

This soft function have the chiral-even and chiral-odd contributions. The chiral-odd term  $S_m$  in this case is not associated with the small current quark mass and therefore we do not expect that  $S_m$  is necessary small. This allows one to combine two collinear operators with different chirality and to obtain the configuration which can not be produced by the hard-rescattering mechanism.

In SCET diagrams this mechanism is realized automatically. In the diagrams in Fig.5(a) and (b) the soft quarks arise between the vertices generated from  $\mathcal{L}_{q\xi}^{(n,1)}$  and  $\mathcal{L}_{q\xi}^{(\bar{n},1)}$ . Such a construction provides that the soft function  $\hat{S}$  is sandwiched between the  $\gamma$ -matrices in the diagram as  $...\not{n}\hat{S}\not{n}...$ . In this case only the chiral odd term  $S_m$  in Eq.(3.58) can survive and as a result only the combination of chiral-even and chiral-odd collinear operators can appear in the resulting SCET-II operator.

Therefore we obtained that there is a soft contribution which is suppressed as  $\Lambda/Q$  comparing to the leading power term. Moreover this contribution does not overlap with any hard configuration and therefore must be well defined in the end-point region. Here we will not discuss this term in detail because we assume that we can not perform the hard-collinear matching at intermediate values of  $Q^2$ .

Consider now the diagram in Fig.5(c) related to the T-product  $\mathcal{C}$  in Eq.(3.52). This diagram involves the higher order vertex generated by the  $\mathcal{O}(\lambda^2)$  Lagrangian  $\mathcal{L}^{(2)}$

$$\mathcal{L}_{q\xi}^{(\bar{n},2)} \sim \bar{\xi}_{\bar{n}}^c \frac{\not{n}}{2} A_{\perp}^c \frac{1}{in \cdot \partial} A_{\perp}^{hc} q. \quad (3.59)$$

Using the SCET counting rules we obtain

$$\mathcal{C} \sim O_n^{(6)} * J_n * q\bar{q} * J_{\bar{n}} * O_{\bar{n}}^{(6)} \sim \lambda^6 \times \lambda^{-4} \times (\lambda^3)^2 \times \lambda^{-2} \times \lambda^6 \sim \lambda^{12}. \quad (3.60)$$

We observe that this example describes the outgoing collinear configuration constructed from the two chiral-odd operators  $O_n^{(6)} O_{\bar{n}}^{(6)}$ . This T-product has the same scaling of order

---

<sup>3</sup>We do not show for simplicity the color indices and the soft gluon lines which necessary for color gauge invariance.



$\lambda^{12}$  as the hard-rescattering contribution with the same collinear operator in Eq.(3.30). Therefore we can conclude that these hard and soft terms can mix or the same overlap. Let us also note that in this case only the chiral-even part of the the soft contribution  $\hat{S}$  (3.58) can contribute. This can be seen from the observation that the vertices (3.59) and  $\mathcal{L}^{(n,1)}$  provide the combination  $\dots \not{A} \hat{S} \not{A} \dots$  in the diagram Fig.5 (c).

The digram in Fig.5(d) is associated with the T-product  $\mathcal{D}$  in Eq.(3.53) and yields an example of the overlap with the chiral-even collinear operators  $O_n^{(8)} O_{\bar{n}}^{(4)}$ . In order to obtain this diagram we used the vertex  $\mathcal{L}_{q\xi}^{(n,2)}$  similar to one in Eq.(3.59) and the interaction with two trnasverse gluons from the leading order term  $\mathcal{L}_{\xi\xi}^{(n,0)}$

$$\left[ \mathcal{L}_{\xi\xi}^{(n,0)} \right]_{\text{int}} \sim \bar{\xi}_n^c g A_{\perp c}^{(n)} \frac{1}{in \cdot \partial} g A_{\perp}^{(n)} \not{n} \xi_n. \quad (3.61)$$

The estimate for this diagram reads

$$\mathcal{D} \sim O_n^{(8)} * J_n * q\bar{q} * J_{\bar{n}} * O_{\bar{n}}^{(4)} \sim \lambda^8 \times \lambda^{-4} \times (\lambda^3)^2 \times \lambda^{-2} \times \lambda^4 \sim \lambda^{12}. \quad (3.62)$$

Therefore this example illustrates another possibility of the overlap between the hard and soft.

We shall not investigate the all possible time-ordered products which provide the overlap between the hard and soft contributions in Eq.(3.45). There are a many of different higher order SCET-I operators which also can be matched onto the collinear operators  $O_c^{(12)}$  as in Eq.(3.30) and providing the scaling behavior of order  $\lambda^{12}$ . Such higher order operators are similar in the structure to the operators  $O^{(3)}$  and  $O_3^{(4)}$  in Eqs. (3.33) and (3.34) but have more gluon fields, as example, we provided the sets of the operators  $O_4^{(5)}$  and  $O^{(5)}$  in Eqs.(3.36) and (3.37).

These operators can also provide the contribution with the operator  $O_c^{(10)}$  describing the collinear sector in SCET-II. Remind that this operator is constructed from the chiral-odd and chiral-even operators and can be obtained only via the soft-quark mechanism as discussed above. However we obtained that all such contributions scale as  $\lambda^{12}$  and therefore they are subleading comparing to contribution arising from the T-products  $\mathcal{A}$  and  $\mathcal{B}$ . As example, consider the SCET-I operator of order  $\lambda^8$  with the following structure

$$O_4^{(8)} = \bar{\chi}_n^c \mathcal{A}_{\perp}^{(n)} \mathcal{A}_{\perp\mu c}^{(\bar{n})} \mathcal{A}_{\perp\nu}^{(\bar{n})} \chi_{\bar{n}}^c. \quad (3.63)$$

It is easy to build the appropriate time-ordered product

$$\begin{aligned} T\{O^{(8)}, \mathcal{L}_{q\xi}^{(n,1)}, \mathcal{L}_{q\xi}^{(\bar{n},1)}\} &\sim O_n^{(4)} * J_n * q\bar{q} * J_{\bar{n}} * O_{\bar{n}}^{(6)} \\ &\sim \lambda^6 \times \lambda^{-2} \times (\lambda^3)^2 \times \lambda^{-2} \times \lambda^4 \sim \lambda^{12}. \end{aligned} \quad (3.64)$$

One of the diagrams describing (3.64) is shown in Fig.6(a).

We also found one more possibility to obtain the soft contribution of order  $\lambda^{10}$  with the collinear operator  $O_c^{(10)}$  defined in Eq.(3.28). Such soft-overlap configuration can be obtained with the SCET-I operator  $O_{\gamma}^{(6)}$  in Eq.(3.41). Appropriate T-product reads (see the diagram in Fig.6(b))

$$T\left\{O_{\gamma}^{(6)}, \mathcal{L}_{\xi\xi}^{(n,0)}, \mathcal{L}_{q\xi}^{(n,1)}\right\} \sim O_{\bar{n}}^{(4)} J_n * q\bar{q} * O_n^{(6)} \sim \lambda^4 \times \lambda^{-6} \times \lambda^6 \times \lambda^6 \sim \lambda^{10}. \quad (3.65)$$



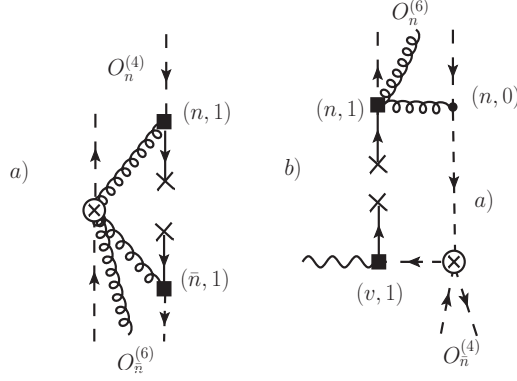


**Figure 6.** Examples of diagrams describing the T-products of certain higher order operators.

However this contribution is subleading in hard  $\alpha_s$  and we neglect it in the leading order approximation.

We obtained that there are many different SCET-I operators which can overlap with the all possible hard contributions. However only the operators  $O^{(3)}$  and  $O_3^{(4)}$  can provide the contribution of order  $\lambda^{10}$  at leading order in hard  $\alpha_s$ . In what follow we assume that the dominant numerical effect is provided by these operators which also have the smallest counting in  $\lambda$  in SCET-I. For brevity we denote the associated operator as

$$O_B = \bar{\chi}_n^C \left( \mathcal{A}_{\perp C}^{(n)} + \mathcal{A}_{\perp C}^{(\bar{n})} \right) \chi_{\bar{n}}^C + (n \leftrightarrow \bar{n}), \quad (3.66)$$

where we assume that the subscript  $C$  denotes collinear or hard-collinear fields. In the subsequent phenomenological description we use the only one SCET-I matrix element

$$\langle p, p' | \bar{\chi}_n^C \left( \mathcal{A}_{\perp C}^{(n)} + \mathcal{A}_{\perp C}^{(\bar{n})} \right) \chi_{\bar{n}}^C + (n \leftrightarrow \bar{n}) | 0 \rangle_{\text{SCET-I}} \sim f_{\pi\pi}(s). \quad (3.67)$$

which describe the two-pion soft-overlap contribution. At large values of  $s$  this SCET FFs behaves as (modulo logarithmic corrections)<sup>4</sup>

$$f_{\pi\pi}(s) \stackrel{s \rightarrow \infty}{\sim} \Lambda^2 \left\{ \frac{\Lambda}{\sqrt{s}} + \alpha \frac{\Lambda^2}{s} \right\}, \quad (3.68)$$

as it follows from the analysis of the T-products  $\mathcal{A} - \mathcal{D}$  carried out above. The two terms in the brackets correspond to the contributions of order  $\lambda^{10}$  and  $\lambda^{12}$ , respectively. The factor  $\alpha$  denotes a simple number.

Contributions of the higher order SCET-I operators  $O^{(\lambda)}$  with  $\lambda > 4$  are stronger suppressed after factorization of the hard modes by the hard scale because these operators have a larger dimension. For instance for the operators in Eq.(3.37)  $\dim[O^{(5)}] = 6$  and therefore

$$\langle p, p' | O^{(5)} | 0 \rangle_{\text{SCET}} \stackrel{s \rightarrow \infty}{\sim} s^2 \lambda^8 \sim \Lambda^4. \quad (3.69)$$

Here we assume that  $O^{(5)}$  is matched onto the operator of order  $\lambda^{12}$  in SCET-II. Taking into account Eq.(3.16) one obtains  $\lambda^8$  for the corresponding contribution in the amplitude.

<sup>4</sup>Taking the matrix element we took into account that the 2-pion state behaves as  $\lambda^{-4}$ , see Eq.(3.16).

The dimensional factor  $\Lambda^n$  in expressions like (3.68) and (3.69) is compensated by inverse power of the hard scale  $Q$  which appears from the hard coefficient function after factorization of the hard modes. In the region of intermediate values of  $Q$  where hard-collinear scale is still not large the contributions of the higher order operators are accompanied by a larger power of the hard scale  $1/Q$ . Perhaps, such contributions are decreasing faster and can be numerically smaller. We postpone the investigation of such corrections for a future.

The subleading hard contribution in Eq.(3.49) has the same order in  $\alpha_s$  as the leading power term but suppressed by power of  $1/Q^2$ . Therefore we expect that this contribution can be small and probably not important. For simplicity we neglect by the hard power subleading terms except one associated with the operator  $O_n^{(6)} O_{\bar{n}}^{(6)}$ .

The total contribution associated with the chiral-odd collinear operator  $O_n^{(6)} O_{\bar{n}}^{(6)}$  includes a specific part which arises due to QCD equations of motions (EOM). These terms are known in the literature as chiral enhanced contributions because of their large numerical normalization factor which is proportional to  $\mu_\pi = m_\pi^2/(m_u + m_d)$ , see Appendix A. The nice feature is that the matrix elements of these contributions can be computed exactly using QCD EOM, see e.g. [42, 43]. In SCET these terms are described by the specific chiral-odd operators with transverse derivative  $\bar{\chi}_n^c \gamma_\perp \gamma_5 \hat{\partial}_\perp / (n \partial) \chi_{\bar{n}}^c$ , see more detail in Appendix A. These operators scale as  $\lambda^6$  similar to the three particle operators  $O_{n,\bar{n}}^{(6)}$  in Eq.(3.30). For simplicity we do not show them in Eq.(3.30) because their contributions are known exactly.

Let us briefly summarise the results of this section. We obtained that at leading order accuracy in hard  $\alpha_s$  the relevant soft contributions to the amplitudes of process  $\gamma\gamma \rightarrow \pi\pi$  are provided by the SCET-I operators  $O^{(i)}$  in Eq.(3.22). Some of these operators are listed in Eqs.(3.32)-(3.36). We also found that in SCET-II these operators can be matched onto collinear operators  $O_c^{(10)}$  and  $O_c^{(12)}$  as in Eqs.(3.28)-(3.30). The obtained soft SCET-II contributions have the same power behavior as the hard terms and therefore we concluded that the hard and soft contributions overlap. This leads to the end-point singularities in the collinear convolution integrals for the soft and hard contributions. In order to avoid uncertainties associated with the regularization in the end-point region we are going to use the physical subtraction scheme which allow to obtain the well defined hard contribution as described in Eq(3.49).

In what follow we assume that the soft-overlap term is dominated by the operator  $O_B$  in Eq.(3.66) which provide the leading power correction. Computing the hard contributions we will take into account only the chiral enhanced contributions. After these simplifications our factorization formula can be written schematically as

$$B_{+\pm}^{(i)}(s, \theta) = C_{+\pm}^{(i)}(s, \theta) * \langle p, p' | O_B | 0 \rangle_{\text{SCET-I}} + \varphi_\chi * H_{+\pm}^{(i)}(s, \theta) * \varphi_\chi. \quad (3.70)$$

Here the asterisks as usually denote the convolution integrals and  $\varphi_\chi$  describes the chiral enhanced DAs. We will compute the hard coefficient functions  $C_{+\pm}^{(i)}$  and  $H_{+\pm}^{(i)}$  below and show that the problem with the end-point singularities in the hard contribution in Eq.(3.70) can be solved in using the approach with physical subtraction scheme as described in this section.

## 4 Calculation of the leading-order coefficient functions for the power subleading contributions

In this section we compute the hard coefficient functions which enter in Eq.(3.70). We show that obtained expression for the soft contribution can be presented in the factorized form as in Eq.(3.46) and therefore one can use the physical subtractions as described above in order to re-express the SCET FF in terms of the physical amplitudes. Then we will obtain the well defined expression for the subleading power corrections  $B_{+\pm}^{(i)}$  which will be used in the subsequent phenomenological analysis.

### 4.1 The soft contribution

First let us clarify the arguments of the fields in the SCET operator  $O_B$  introduced in Eq.(3.66). We assume that the fields are multipole expanded in the position space.<sup>5</sup> We define this operator as

$$O_B(\lambda) = \bar{\chi}_n^C(0) \left( \mathcal{A}_{\perp C}^{(n)}(\lambda \bar{n}) + \mathcal{A}_{\perp C}^{(\bar{n})}(\lambda n) \right) \chi_{\bar{n}}^C(0), \quad (4.1)$$

where, remind,  $\bar{\chi}_n^C$  and  $\mathcal{A}_{\perp C}$  are defined in Eqs.(3.6) and (3.7). This operator depend on the relative light-cone distance  $\lambda$  between the hard-collinear quark and gluon. Performing the Fourier transformation with respect to  $\lambda$  one introduces the conjugate variable  $\tau$  which can be interpreted as a fraction of the total hard-collinear momentum carried by gluon. It is convenient to introduce the following momentum space representation

$$\mathcal{A}_{\mu C}^{(n)}(\tau) = \int \frac{d\lambda}{2\pi} P'_+ e^{-i\lambda P'_+ \tau} \mathcal{A}_{\mu C}^{(n)}(\lambda \bar{n}), \quad (4.2)$$

where  $P'$  denote the momentum operator in the  $n$ -collinear sector. The similar expression holds also for the  $\mathcal{A}_{\mu C}^{(\bar{n})}$ . Using this compact notation one can define the matrix element directly in the momentum space. Hence we define the SCET-I operator as

$$O_B(\tau) = \bar{\chi}_n^C(0) \left( \mathcal{A}_{\perp C}^{(n)}(\tau) + \mathcal{A}_{\perp C}^{(\bar{n})}(\tau) \right) \chi_{\bar{n}}^C(0). \quad (4.3)$$

This allows us to introduce the parametrization of the SCET-I matrix element as

$$\left\langle \pi^a(p), \pi^b(p') | O_B(\tau) | 0 \right\rangle_{\text{SCET-I}} = \delta^{ab} (4\pi f_\pi)^2 f_{\pi\pi}(\tau, s). \quad (4.4)$$

Here we used the dimensional factor  $(4\pi f_\pi)^2$  just for convenience. The dimensionless SCET FF  $f_{\pi\pi}(\tau, s)$  depends on the collinear fraction  $\tau$  and hard scale  $s$ . and might be a complex function. This FF depends also from the factorization scale which is not shown for simplicity. The evolution of the operators like  $O_B(\tau)$  has been studied in Refs.[44, 45]. In Eq.(4.4) we assume that the operator  $O_B(\tau)$  is the singlet in the flavor

$$O_B(\tau) \sim \bar{u}u + \bar{d}d. \quad (4.5)$$

---

<sup>5</sup> Assuming that SCET-I Lagrangian is constructed from the hard-collinear and collinear fields one comes to the SCET Lagrangian which has no homogeneous power counting. Such intermediate formulation have certain problems with the treatment of gauge invariance, see discussion in Ref.[38]. Here we do not consider the full SCET-II matching and therefore we assume that these subtleties can be ignored.

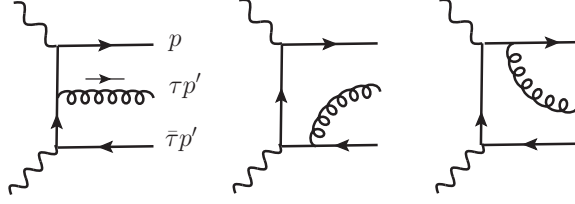


**Figure 7.** The set of the diagrams required for the matching of T-product of the electromagnetic currents onto SCET-I operator  $O_B(\tau)$ . The crossed diagrams are not shown for the brevity. We also show only the diagrams for the case  $\bar{\chi}_n \not{A}_\perp^{(\bar{n})} \chi_{\bar{n}}$ . The diagrams describing the other configurations are similar. In the first diagram we used  $\bar{\tau} \equiv 1 - \tau$ .

The similar operator with isospin  $I = 1$  can not contribute to our process due to  $C$ -parity. This allows one to conclude that such soft contribution can be relevant only for the isoscalar amplitudes  $B_{+\pm}^{(0)}$ . Therefore the factorization of the soft contributions can be written as

$$B_{+\pm}^{(0,s)}(s, \theta) = (4\pi f_\pi)^2 \int_0^1 d\tau C_{+\pm}^{(0)}(s, \theta, \tau) f_{\pi\pi}(\tau, s), \quad (4.6)$$

$$B_{+\pm}^{(3,s)}(s, \theta) = \mathcal{O}(\alpha_s). \quad (4.7)$$

Notice, that from the general equation (4.6) one can not see a possibility to factorize the  $\theta$ -dependence as it assumed in Eq.(3.46).

In order to compute the leading order coefficient functions  $C_{+\pm}^{(0,s)}$  one has to compute the tree level diagrams shown in Fig.7. This computation is quite standard and we provide the resulting expressions without discussion of the technical details. Our results read

$$B_{++}^{(0,s)}(s, \eta) = - (e_u^2 + e_d^2) \frac{(4\pi f_\pi)^2}{s} \frac{4}{1 - \eta^2} \int_0^1 d\tau \frac{\tau}{1 - \tau} f_{\pi\pi}(\tau, s), \quad (4.8)$$

$$B_{+-}^{(0,s)}(s, \eta) = - 2(e_u^2 + e_d^2) \frac{(4\pi f_\pi)^2}{s} \frac{3 - \eta^2}{1 - \eta^2} \int_0^1 d\tau f_{\pi\pi}(\tau, s), \quad (4.9)$$

where we introduced the short notation

$$\eta \equiv \cos \theta. \quad (4.10)$$

Both helicity amplitudes in Eqs.(4.8) and (4.9) are defined in terms of the same SCET FF  $f_{\pi\pi}$  but the convolution integrals are different. We also obtained a bit different  $\eta$ -dependence in the each case. From Eqs.(4.8) and (4.9) we observe that the  $\eta$ -dependent factors are factorized from the integration over collinear fraction  $\tau$ . Therefore introducing the two independent SCET FFs as

$$\Phi_{++}(s) = \int_0^1 d\tau \frac{\tau}{1 - \tau} f_{\pi\pi}(\tau, s), \quad (4.11)$$

$$\Phi_{+-}(s) = \int_0^1 d\tau f_{\pi\pi}(\tau, s). \quad (4.12)$$

we can present the amplitudes  $B_{+\pm}^{(0,s)}$  in the factorized form as in Eq.(3.49).

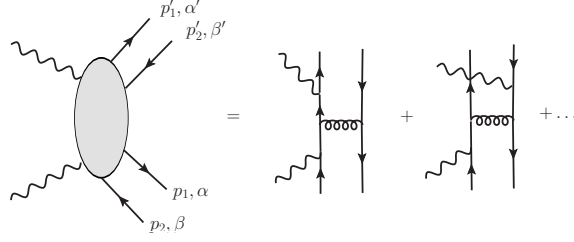


**Figure 8.** Graphical representation of the function  $D_{ab}^{\mu\nu}(p_i, p'_i)$  defined in Eq.(4.13).

## 4.2 The subleading hard contribution

In this case as we explained in Sec.3 we are going to compute only the chiral enhanced terms. The diagrams which we need are similar to those in Fig.1 but with the appropriate twist-3 projections for the pion DAs. In order to compute these hard amplitudes we use the twist-3 projection technique suggested in Refs.[42, 46]. Therefore in the compact form the expressions which we have to compute can be written as

$$\delta^{ab} B_{+\pm}^{(0,h)} + \delta^{a3} \delta^{b3} B_{+\pm}^{(3,h)} = \frac{(f_\pi \mu_\pi)^2}{16} \int_0^1 dx \hat{M}_{\beta'\alpha'}(x, p') \int_0^1 dy \hat{M}_{\beta\alpha}(y, p) \times \left[ 2M_{1,2}^{\mu\nu} D_{ab}^{\mu\nu}(p_i, p'_i) \right]_{\alpha'\beta; \alpha\beta'}. \quad (4.13)$$

Here  $D_{ab}^{\mu\nu}(p_i, p'_i)$  denotes the sum of all relevant diagrams describing the hard subprocess  $\gamma\gamma \rightarrow (q\bar{q})_n + (q\bar{q})_{\bar{n}}$ . The external momenta of the outgoing quarks are shown in Fig.8. Their light-cone expansions read

$$p_1 \simeq yp + r_\perp, \quad p_2 \simeq \bar{y}p - r_\perp, \quad (4.14)$$

$$p'_1 \simeq xp' + k_\perp, \quad p'_2 \simeq \bar{x}p' - k_\perp. \quad (4.15)$$

The twist-3 quark projectors  $\hat{M}$  in Eq.(4.13) are given by

$$\hat{M}_{\alpha\beta}(y, p) = \phi_p(y) [\gamma_5]_{\beta\alpha} - p_\lambda \left[ \sigma^{\lambda\rho} \gamma_5 \right]_{\beta\alpha} \frac{i}{6} \left[ \frac{n^\rho}{(p \cdot n)} \phi'_\sigma(y) - \phi_\sigma(y) \frac{\partial}{\partial r_\perp^\rho} \right], \quad (4.16)$$

$$\hat{M}_{\beta'\alpha'}(x, p') = \phi_{p'}(x) [\gamma_5]_{\beta'\alpha'} - p'_\lambda \left[ \sigma^{\lambda\rho} \gamma_5 \right]_{\beta'\alpha'} \frac{i}{6} \left[ \frac{\bar{n}^\rho}{(p' \cdot \bar{n})} \phi'_\sigma(x) - \phi_\sigma(x) \frac{\partial}{\partial k_\perp^\rho} \right]. \quad (4.17)$$

Here for the DA's  $\phi_{p,\sigma}$  we use only the chiral enhanced pieces

$$\phi_p(x) = 1, \quad \phi_\sigma(x) = 6x\bar{x}, \quad \phi'_\sigma(x) = 6(1 - 2x). \quad (4.18)$$

The expressions in Eq's.(4.16) and (4.17) includes the differentiations with respect to the relative transverse momenta  $r_\perp$  and  $k_\perp$  of the quarks and antiquarks. Only after the differentiation one can put  $r_\perp = k_\perp = 0$ . In order to compute the expression in Eq.(4.13) we used the package *FeynCalc* [47]. Performing this calculation we obtained

$$B_{++}^{(0,h)}(s, \eta) \simeq B_{++}^{(3,h)}(s, \eta) \simeq 0, \quad (4.19)$$

$$B_{+-}^{(0,h)}(s, \eta) = \frac{\alpha_s}{4\pi} \frac{C_F}{N_c} \frac{(4\pi f_\pi)^2}{s} \frac{\mu_\pi^2}{s} \left\{ (e_u^2 + e_d^2) \frac{(3 - \eta^2)}{(1 - \eta^2)} I_s + \frac{2e_u e_d}{(1 - \eta^2)} I(\eta) \right\}, \quad (4.20)$$

$$B_{+-}^{(3,h)}(s, \eta) = \frac{\alpha_s}{4\pi} \frac{C_F}{N_c} \frac{(4\pi f_\pi)^2}{s} \frac{\mu_\pi^2}{s} \frac{(e_u - e_d)^2}{(1 - \eta^2)} I(\eta), \quad (4.21)$$

with  $C_F = \frac{N_c^2 - 1}{2N_c}$ ,

$$I(\eta) = 8 - 4\eta \ln \left[ \frac{1 + \eta}{1 - \eta} \right] + 2(3 - \eta^2) \left\{ \text{Li} \left[ \frac{1 + \eta}{2} \right] + \text{Li} \left[ \frac{1 - \eta}{2} \right] - \frac{2\pi^2}{3} - \ln^2 \frac{1 + \eta}{1 - \eta} + \frac{1}{2} \left( \ln^2 \frac{1 + \eta}{2} + \ln^2 \frac{1 - \eta}{2} \right) \right\}, \quad (4.22)$$

and the singular integral

$$I_s = \int dx dy \left( \frac{1}{y\bar{x}} + \frac{1}{x\bar{y}} \right). \quad (4.23)$$

Here  $\text{Li}[z]$  denotes the Spence function (dilogarithm) defined by

$$\text{Li}(z) = - \int_0^z dt \frac{\ln(1 - t)}{t}. \quad (4.24)$$

We obtained that there is no chiral enhanced corrections to the helicity amplitudes  $B_{++}^{(i,h)}$ . We checked that these amplitudes obtain the corrections from the twist-3 three-particle DA but we neglected these contributions assuming they are small, see discussion in Appendix A.

The integral  $I_s$  in Eq.(4.21) is real and has the logarithmic end-point divergencies as expected. We do not write any explicit regularization for simplicity. Notice that the  $\theta$ -dependence in front this integral in Eq.(4.20) is exactly the same as in the soft contribution  $B_{+-}^{(0,s)}$  in Eq.(4.9). This observation is very important in order to proceed with the subtraction of the singular integral as described below.

The expression  $I(\eta)$  arises from the other finite convolution integral and associated with the diagrams where the photons couple to quark and antiquark lines. These terms are finite and corresponding convolution integrals can be computed explicitly. Taking into account that we will need this result at small  $\eta \sim 0$  ( $\theta \sim 90^\circ$ ) we obtain

$$I(\eta \rightarrow 0) = 8 - 3\pi^2 + \eta^2(\pi^2 - 20) + \mathcal{O}(\eta^4). \quad (4.25)$$

### 4.3 Subleading amplitudes in the physical subtraction scheme

Summing the hard and soft contributions which were computed above we find

$$B_{+-}^{(0)}(s, \eta) \simeq -2(e_u^2 + e_d^2) \frac{(4\pi f_\pi)^2}{s} \frac{3 - \eta^2}{1 - \eta^2} \Phi_{+-}(s) + \frac{\alpha_s}{4\pi} \frac{C_F}{N_c} \frac{(4\pi f_\pi)^2}{s} \frac{\mu_\pi^2}{s} \left\{ (e_u^2 + e_d^2) \frac{(3 - \eta^2)}{(1 - \eta^2)} I_s + \frac{2e_u e_d}{(1 - \eta^2)} I(\eta) \right\} \quad (4.26)$$

$$B_{++}^{(0)}(s, \eta) \simeq B_{++}^{(0,s)}(s, \theta) = - (e_u^2 + e_d^2) \frac{(4\pi f_\pi)^2}{s} \frac{4}{1 - \eta^2} \Phi_{++}(s), \quad (4.27)$$

$$B_{++}^{(3)}(s, \eta) \simeq 0, \quad (4.28)$$

$$B_{+-}^{(3)}(s, \eta) \simeq B_{+-}^{(3,h)}(s, \eta) = \frac{\alpha_s}{4\pi} \frac{C_F}{N_c} \frac{(4\pi f_\pi)^2}{s} \frac{\mu_\pi^2}{s} \frac{(e_u - e_d)^2}{(1 - \eta^2)} I(\eta). \quad (4.29)$$

The expression for the  $B_{+-}^{(0)}(s, \eta)$  in Eq.(4.26) includes the divergent integral in the hard term and therefore we apply the subtraction method described in Sec.3. As subtraction point we take the value  $\theta_0 = 90^\circ$  that corresponds to  $\eta = \cos \theta_0 = 0$ . Then from Eq.(4.26) one obtains

$$\Phi_{+-}(s) = -\frac{1}{(e_u^2 + e_d^2)} \frac{1}{6} \frac{s}{(4\pi f_\pi)^2} \quad (4.30)$$

$$\left[ B_{+-}^{(0)}(s, 0) - \frac{\alpha_s}{4\pi} \frac{C_F}{N_c} \frac{(4\pi f_\pi)^2}{s} \frac{\mu_\pi^2}{s} \{3(e_u^2 + e_d^2) I_s + 2e_u e_d I(0)\} \right]. \quad (4.31)$$

Substituting this expression into Eq.(4.26) for arbitrary  $\eta$  we obtain

$$B_{+-}^{(0)}(s, \eta) = \frac{3 - \eta^2}{1 - \eta^2} \frac{1}{3} B_{+-}^{(0)}(s, 0) + \Delta_{+-}^{(0)}(s, \eta). \quad (4.32)$$

with the hard contribution

$$\Delta_{+-}^{(0)}(s, \eta) = \frac{\alpha_s}{2\pi} \frac{C_F}{N_c} \frac{(4\pi f_\pi)^2}{s} \frac{\mu_\pi^2}{s} \frac{e_u e_d}{(1 - \eta^2)} \left\{ I(\eta) - (3 - \eta^2) \frac{1}{3} I(0) \right\} \quad (4.33)$$

We see that the divergent integral  $I_s$  cancel as expected and we obtain the equation which describes the amplitudes up to one unknown factor  $B_{+-}^{(0)}(s, 0)$ . Because the  $\eta$ -dependence is determined we can compare the obtained result with the data at fixed energy.

Using the same method with  $\theta_0 = 90^\circ$  for the amplitude  $B_{++}^{(0)}$  yields

$$B_{++}^{(0)}(s, \eta) \simeq \frac{B_{++}^{(0)}(s, 0)}{1 - \eta^2}. \quad (4.34)$$

Remind that in this formula we neglected the hard corrections assuming that they are small. To the same reason the amplitude  $B_{++}^{(3)}$  is also negligible.

It is interesting to compare the hard contributions associated with the leading twist and subleading chiral enhanced corrections. In Fig.9 we show the ratios of the  $\Delta_{+-}^{(0)}/A_{+-}^{(0)}$  (left) and  $B_{+-}^{(3)}/A_{+-}^{(3)}$  (right) as functions of  $\cos \theta$  for two different values of  $s$ . In order to compute these ratios we used BA-set for the leading twist pion DA, see Eq.(2.34). The renormalization scale  $\mu_R$  for the running coupling and for the quark masses is fixed to be  $\mu_R = 0.8W$  GeV.

The ratio  $\Delta_{+-}^{(0)}/A_{+-}^{(0)}$  is small, and tends to zero when  $\cos \theta \rightarrow 0$ . This is direct consequence of the our subtraction scheme with subtractions at  $\theta_0 = 0$  that ensures  $\Delta_{+-}^{(0)}(s, \eta \rightarrow 0) \rightarrow 0$ . Therefore in this case the numerical effect from the chiral enhanced power correction is very small. But the behavior of the ratio  $B_{+-}^{(3)}/A_{+-}^{(3)}$  is very different. In this case the absolute value of the subleading amplitude is comparable to the leading one providing the large effect. Even at  $s = 16\text{GeV}^2$  the effect from the chiral power correction

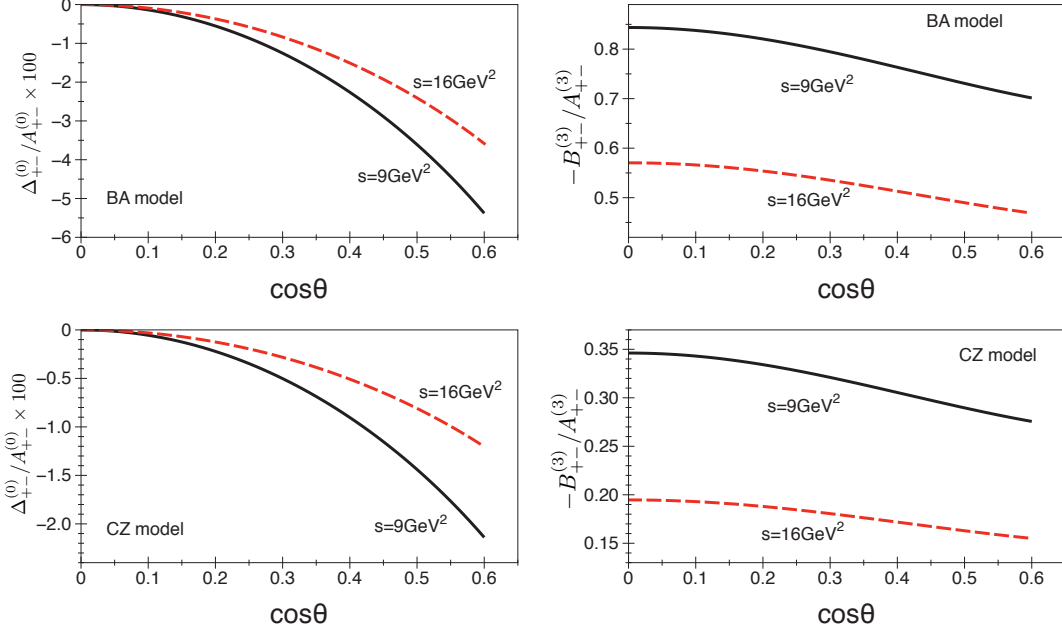


**Figure 9.** The ratios of the hard subleading power amplitude to the leading power contribution. The first (second) line shows the plots for the BA(CZ)-model of pion DA.

is of order 40 – 50%. Taking into account that  $B_{+-}^{(3)}$  and  $A_{+-}^{(3)}$  have the opposite relative sign one finds that the value of the sum  $B_{+-}^{(3)} + A_{+-}^{(3)}$  is strongly reduced. Therefore the effect of the chiral power correction for this amplitude is large and must be taken into account.

If one uses CZ-model for the pion DA ( $\mu_R = 1.3\text{GeV}$ ) then the relative value of the hard subleading corrections is considerably smaller because the absolute value of the leading power contribution is larger. The result for the ratios in this case are shown in the bottom line in Fig.9.

Summarizing, we obtained the expressions for the subleading amplitudes which depend on the two unknown functions  $B_{+-}^{(0)}(s, 0)$  and  $B_{++}^{(0)}(s, 0)$  which describe the soft-overlap contribution in the physical subtraction scheme. Below we use these results together with the leading power expressions  $A_{\pm\pm}^{(i)}$  in order to perform the phenomenological analysis of the existing data.



## 5 Phenomenological analysis

Using the obtained results we write the expression for the pion production cross sections in the following form

$$\begin{aligned} \frac{d\sigma^{\pi^+\pi^-}}{d\cos\theta} = \frac{\pi\alpha^2}{16s} & \left( \frac{|B_{++}^{(0)}(s,0)|^2}{(1-\eta^2)^2} + \left( \frac{1-\eta^2/3}{1-\eta^2} \right)^2 |B_{+-}^{(0)}(s,0)|^2 + |A_{++}^{(0)}|^2 + |A_{+-}^{(0)} + \Delta_{+-}^{(0)}|^2 \right. \\ & \left. + 2A_{++}^{(0)} \frac{\text{Re}[B_{++}^{(0)}(s,0)]}{1-\eta^2} + 2\frac{1-\eta^2/3}{1-\eta^2} (A_{+-}^{(0)} + \Delta_{+-}^{(0)}) \text{Re}[B_{+-}^{(0)}(s,0)] \right), \end{aligned} \quad (5.1)$$

$$\begin{aligned} \frac{d\sigma^{\pi^0\pi^0}}{d\cos\theta} = \frac{\pi\alpha^2}{32s} & \left( \frac{|B_{++}^{(0)}(s,0)|^2}{(1-\eta^2)^2} + \left( \frac{1-\eta^2/3}{1-\eta^2} \right)^2 |B_{+-}^{(0)}(s,0)|^2 \right. \\ & + |A_{+-}^{(0)} + \Delta_{+-}^{(0)} + A_{+-}^{(3)} + B_{+-}^{(3,h)}|^2 \\ & \left. + 2\frac{1-\eta^2/3}{1-\eta^2} (A_{+-}^{(0)} + \Delta_{+-}^{(0)} + A_{+-}^{(3)} + B_{+-}^{(3,h)}) \text{Re}[B_{+-}^{(0)}(s,0)] \right). \end{aligned} \quad (5.2)$$

Remind that  $\eta \equiv \cos\theta$ , the expressions describing the leading power contributions  $A_{\pm\pm}^{(i)}$  can be found in Eq's.(2.25)-(2.27), the subleading amplitudes  $B_{+-}^{(3,h)}$  and  $\Delta_{+-}^{(0)}$  are given in Eq's.(4.29) and (4.33), respectively. Here we used that all these hard contributions are real and therefore their interference with the unknown amplitudes depends only from the real parts  $\text{Re}[B_{+-}^{(0)}(s,0)]$  and  $\text{Re}[B_{+-}^{(0)}(s,0)]$ . All the amplitudes are functions of energy  $s$  and the scattering angle  $\theta$ . The expressions in Eqs.(5.1) and (5.2) will be used in order to perform the analysis of BELLE data [6, 7] for the differential cross sections in the region  $W = 3 - 4\text{GeV}$ .

Using the  $\cos\theta$ -dependence one can try to fit these data in order to extract values of the unknown amplitudes  $B_{\pm\pm}^{(0)}(s,0)$ . In the subsequent analysis we assume that the dominant contribution in the unknown amplitudes  $B_{\pm\pm}^{(0)}(s,0)$  is given by the real part and therefore we can neglect the effect produced by the imaginary part

$$\text{Im } B_{\pm\pm}^{(0)}(s,0) \approx 0. \quad (5.3)$$

In this case we have only the two unknown real parameters  $B_{\pm\pm}^{(0)}(s,0)$  at each fixed energy  $s$ . The resulting expressions for the cross sections depend also from the model for the pion DA. We consider two cases when pion DA is described by BA and CZ-models, see Eqs.(2.34) and (2.36). Using the other models described in Eqs.(2.33) and (2.35) gives results which are close to one obtained with the BA-model.

Using the expressions in Eqs.(5.1),(5.2) one can study the behavior of the cross section with respect to scattering angle  $\theta$  at fixed energy. This behavior is given by the coefficients in front of unknown amplitudes  $B_{\pm\pm}^{(0)}(s,0)$ . We easily observe that the ratio of the coefficients in front of the quadratical terms  $|B_{\pm\pm}^{(0)}|^2$  in Eqs.(5.1) and (5.2) is given

by  $(1 - \eta^2/3)^2 \leq 0.774$  in the region where  $|\eta| \leq 0.6$ . It is clear that this difference is negligible when  $\eta$  is small and becomes the largest when  $\eta = \eta_{\max} = 0.6$ . Such relatively small deviation from  $1/(1 - \eta^2)$  behavior can only be visible if the value of the amplitude  $B_{+-}^{(0)}$  is quite large.

The linear in  $B_{+\pm}$  terms in Eqs.(5.1),(5.2) can also provide a significant numerical effect. Let us consider their behavior in  $\cos \theta$ . From Eq.(2.25) one finds that  $A_{++}^{(0)} \sim 1/(1 - \eta^2)$ . The combination  $(1 - \eta^2/3) (A_{+-}^{(0)} + \Delta_{+-}^{(0)})$  which inter in Eq.(5.1) also behaves as  $1/(1 - \eta^2)$ . In Fig.10 we plot this linear term

$$\rho_{+-}(s, \eta) = (1 - \eta^2/3) (A_{+-}^{(0)}(s, \eta) + \Delta_{+-}^{(0)}(s, \eta)), \quad (5.4)$$

and the approximate expression which is given

$$\tilde{\rho}_{+-}(s, \eta) \simeq \frac{\rho_{+-}(s, 0)}{1 - \eta^2}. \quad (5.5)$$

at fixed  $W = 3\text{GeV}$ . From this figure one can see that the difference between two expressions is quite small for the all models of pion DA. This picture does not change in the region of energy  $W = 3 - 4\text{GeV}$ . Therefore to a very good accuracy one can expect that

$$\frac{d\sigma^{\pi^+\pi^-}}{d\cos\theta} \sim \frac{1}{(1 - \eta^2)^2}. \quad (5.6)$$

This consideration allows us to conclude that the fitting the differential cross section  $d\sigma^{\pi^+\pi^-}/d\cos\theta$  one can not perform the extraction of the two amplitudes  $B_{+\pm}^{(0)}$ .

The qualitative observation (5.6) is in agreement with experimental data [6]. The behavior of the cross section as in Eq.(5.6) was also obtained in handbag model approach Ref.[17]. However within this framework  $B_{++}^{(i)} = 0$  that is not agree with the our result in Eq.(5.1).

For the neutral pion cross sections in Eq.(5.2) the linear contribution depends only from the amplitude  $B_{+-}^{(0)}$  and the corresponding hard coefficients reads

$$\lambda_{+-}(s, \eta) = A_{+-}^{(0)}(s, \eta) + \Delta_{+-}^{(0)}(s, \eta) + A_{+-}^{(3)}(s, \eta) + B_{+-}^{(3,h)}(s, \eta). \quad (5.7)$$

The  $\eta$ -dependence of this expression deviates from the simple  $1/(1 - \eta^2)$  behavior. In Fig.10 we show the exact value  $\lambda_{+-}(s, \eta)$  in comparison with the approximation

$$\tilde{\lambda}_{+-}(s, \eta) = \frac{\lambda_{+-}(s, 0)}{(1 - \eta^2)}. \quad (5.8)$$

We observe that in this case the deviation from the profile  $1/(1 - \eta^2)$  reaches 30% for the CZ-model. Therefore if the value of the amplitude  $B_{+-}^{(0)}$  is relatively large then the corresponding linear term in the neutral pion cross section can provide a sizable numerical effect. In this case the separation of the two amplitudes using the angular behavior can be performed in a better way.

Let us also notice that for the boundary value  $\eta_{\max} = 0.6$  and the energy  $W = 3-4\text{GeV}$  the values of  $|t| = |u| = 1.8 - 3.2\text{GeV}^2$ . Phenomenologically such values of  $t$  and  $u$

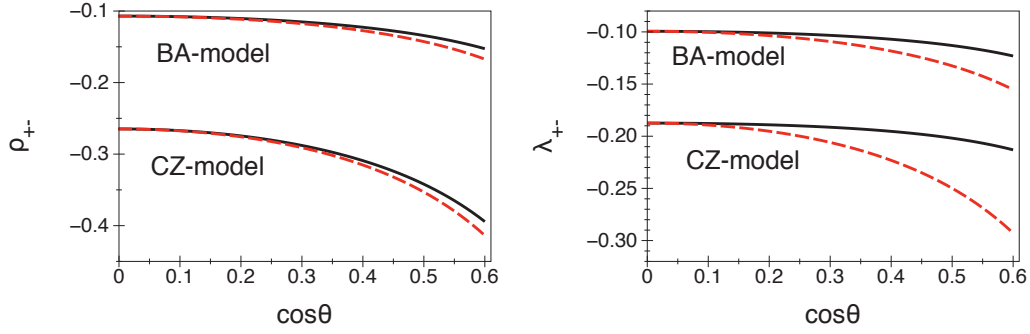


**Figure 10.** The linear coefficients  $\rho_{+-}$  defined in Eq.(5.4) (left figure) and  $\lambda_{+-}$  defined in Eq.(5.7) (right figure) as a functions of  $\eta = \cos \theta$  at fixed energy  $W = 3\text{GeV}$ . The exact values of these coefficients are shown by solid black lines. The approximations  $\tilde{\rho}_{+-}$  (5.5) and  $\tilde{\lambda}_{+-}$  (5.8) are given by dashed red lines. For the numerical calculations of the amplitudes we used the same input parameters as in Figs.9

can be considered as pre-asymptotic and one can not exclude a substantial numerical corrections associated with the different next-to-leading contributions. Therefore we can expect that the accuracy of our approach is worse near the boundary region  $\eta_{\text{max}} \sim 0.6$  and  $W = 3 - 4\text{GeV}$ .

One can easily observe from Eqs.(5.1) and (5.2) that keeping only the quadratical in  $B_{+\pm}^{(0)}$  terms (i.e. neglecting the *all* known hard contributions) one finds that the ratio does not depend on the angle  $\theta$  and

$$\left[ \frac{d\sigma^{\pi^0\pi^0}}{d\cos\theta} / \frac{d\sigma^{\pi^+\pi^-}}{d\cos\theta} \right]_{\text{soft}} = \frac{1}{2}. \quad (5.9)$$

The deviation from this value in the present formalism can be explained only by the presence of the interference of the computed hard contributions  $A_{+\pm}^{(i)}$ ,  $B_{+-}^{(3,h)}$  with the unknown soft amplitudes  $B_{+\pm}^{(0)}(s, 0)$ .

### 5.1 Analysis of BELLE data using the BA-model of pion DA

We start the comparison with the data using as input the BA-model for the pion DA, see Eq.(2.34). Computing the cross sections we use for the hard scale the value  $\mu_R = 0.8W$ . We use this scale in order to compute the running coupling  $\alpha_s(\mu_R)$ , the moments  $a_{2n}(\mu_R)$  and quark masses in expression for  $\mu_\pi$  in Eq.(A.4).

In order to see the numerical effect from the subleading corrections consider numerical values of the different contributions in the cross sections. Taking  $W = 3.05\text{GeV}$ ,  $\cos \theta =$

0.05 we obtain

$$\left(\frac{d\sigma^{\pi^+\pi^-}}{d\cos\theta}\right)_{\text{LT}} = 0.0283, \quad \left(\frac{d\sigma^{\pi^+\pi^-}}{d\cos\theta}\right)_{\text{exp}} = 0.312 \pm 0.039, \quad (5.10)$$

$$\left(\frac{d\sigma^{\pi^0\pi^0}}{d\cos\theta}\right)_{\text{LT}} = 0.0014, \quad \left(\frac{d\sigma^{\pi^0\pi^0}}{d\cos\theta}\right)_{\text{exp}} = 0.078 \pm 0.025, \quad (5.11)$$

$$\frac{d\sigma^{\pi^+\pi^-}}{d\cos\theta} = 0.879|B_{++}^{(0)}|^2 + 0.878|B_{+-}^{(0)}|^2 - 0.259B_{++}^{(0)} - 0.180B_{+-}^{(0)} + 0.0283, \quad (5.12)$$

$$\frac{d\sigma^{\pi^0\pi^0}}{d\cos\theta} = 0.440|B_{++}^{(0)}|^2 + 0.439|B_{+-}^{(0)}|^2 - 0.083B_{+-}^{(0)} + 0.004. \quad (5.13)$$

Here the subscript “LT” denotes the leading twist approximation. For comparison we also showed in Eqs.(5.10) and (5.11) the experimental values obtained in Refs.[6, 7].

Comparing the numerical values in Eq.(5.11) and (5.13) one can observe that hard subleading contribution  $B_{+-}^{(3,h)}$  for the  $\pi^0\pi^0$  channel provides the sizable numerical effect comparing to leading twist result. However the absolute value of the total effect is very small in comparison of experimental value in Eq.(5.11). The similar picture holds also for the other values of  $\theta$ . Therefore we conclude that we can reproduce the data only if the values of the amplitudes  $B_{+\pm}^{(0)}$  are quite large. If the obtained description of the cross section angular behavior is consistent with the data then we can extract the values of the amplitudes  $B_{+\pm}^{(0)}$ .

In Fig.11 and Fig.12 we present the results of the fits of the BELLE data [6, 7] for the charged and neutral pion, respectively. Notice, that the data for neutral pion production in the region  $W = 3.3 - 3.6\text{GeV}$  are absent because of charmonium production. Therefore in this region we can not perform the two-parameter fit with respect to  $B_{+\pm}^{(0)}(s, 0)$ . The results of the two-parameter fit of the both data sets (the charged and neutral pions) are shown by dashed lines in Figs.11 and 12. In Table 1 we present the results for the extracted amplitudes  $B_{+\pm}^{(0)}(s, 0)$  in the each energy interval. We observe that in the region

**Table 1.** The values of the  $B_{+\pm}^{(0)}(s, 0)$  obtained from the two-parameter fit of the cross sections measured by BELLE collaboration [6, 7]. The given reduced values of  $\chi^2$  were computed with dof= 16.

$W, \text{ GeV}$	$B_{++}^{(0)}(s, 0)$	$B_{+-}^{(0)}(s, 0)$	$\chi^2/\text{dof}$
3.05	$-0.47 \pm 0.16$	$0.068 \pm 2.96$	2.32
3.15	$-0.44 \pm 0.17$	$0.057 \pm 2.68$	1.89
3.65	$-0.260 \pm 0.34$	$-0.003 \pm 1.7$	0.98
3.75	$-0.22 \pm 0.21$	$-0.1 \pm 0.38$	1.28
3.85	$-0.17 \pm 0.12$	$0.25 \pm 0.14$	0.67
3.95	$-0.18 \pm 0.11$	$0.15 \pm 0.26$	0.58

$W = 3.05 - 3.65\text{GeV}$  the absolute value of  $|B_{+-}^{(0)}|$  is quite small. As a result the angular

separation works bad and the standard errors for the value  $B_{+-}^{(0)}$  are always very large. It demonstrates that in this case the application of the expressions in Eqs.(5.1) and (5.2) for the fit of the data does not allow one to perform the separation of the unknown amplitudes and to extract their values with a reasonable accuracy. For that purpose one needs some

**Table 2.** Results for the amplitude  $B_{++}^{(0)}(s, 0)$  obtained from the one-parameter fit of the BELLE data [6] for charged pion production.

$W, \text{ GeV}$	3.05	3.15	3.25	3.35	3.45
$B_{++}^{(0)}(s, 0)$	$-0.48 \pm 0.02$	$-0.44 \pm 0.02$	$-0.39 \pm 0.02$	$-0.35 \pm 0.03$	$-0.30 \pm 0.03$
$\chi^2/\text{dof}$	1.5	2.3	2.5	2.0	1.8

$W, \text{ GeV}$	3.55	3.65	3.75	3.85	3.95	4.05
$B_{++}^{(0)}(s, 0)$	$-0.27 \pm 0.03$	$-0.29 \pm 0.04$	$-0.27 \pm 0.03$	$-0.23 \pm 0.03$	$-0.20 \pm 0.03$	$-0.15 \pm 0.04$
$\chi^2/\text{dof}$	1.9	0.8	0.8	0.8	0.4	3.6

additional information.

Using the results of the two-parameter fit we can conclude that, at least, qualitatively one can assume that  $|B_{++}^{(0)}| \gg |B_{+-}^{(0)}|$ . For larger values of energy  $W \geq 3.75 \text{ GeV}$  the central value of  $B_{+-}^{(0)}$  is already quite large but the error bars of the data are also large. Guided by the results from the region  $W = 3.05 - 3.65 \text{ GeV}$  we consider a simple model assuming

$$B_{+-}^{(0)} \simeq 0. \quad (5.14)$$

In this case one can perform more simple one-parameter fit of the charged pion cross section data and to define the value of  $B_{++}^{(0)}$ . Then using this value one can compute of the neutral pion cross section and compare with the data. The obtained results are shown in Fig.11 and Fig.12 by solid line. We observe that the difference between one- and two-parameter fits is small. Taking into account the accuracy of the leading order contribution (in  $\alpha_s$ ) we can conclude that in both cases the obtained description is reliable.

In Table 2 we present the results for the values  $B_{++}^{(0)}$  obtained from the one-parameter fit. One can see that one-parameter fit is much better, it has better  $\chi^2$  and relatively small standard error. However this estimates are no longer unbiased and the small error bars can also arise due to the effect of underfitting<sup>6</sup>. Nevertheless we consider that this model is interesting providing the simple scenario which describes the data.

Substituting the values  $B_{++}^{(0)} = -0.48$ ,  $B_{+-}^{(0)} \simeq 0$  in the expression in Eqs. (5.12) we obtain

$$\frac{d\sigma^{\pi^+\pi^-}}{d\cos\theta}(3.05 \text{ GeV}, \cos\theta = 0.05) = 0.879|B_{++}^{(0)}|^2 - 0.259B_{++}^{(0)} + 0.0283 \quad (5.15)$$

$$= 0.19B_{++}^2 + 0.12B_{++} + 0.0283 \simeq 0.34, \quad (5.16)$$

---

<sup>6</sup>The author thanks to M.Distler for the discussion of this moment.

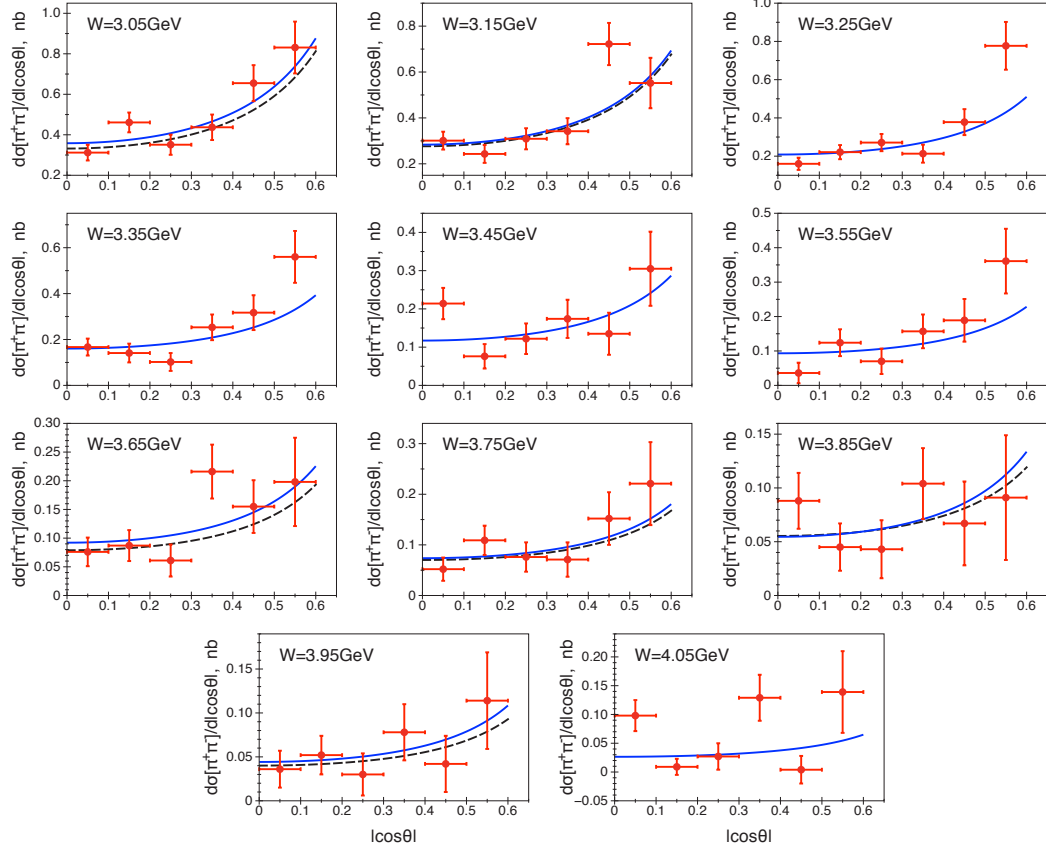


**Figure 11.** Results of the fit for the charged pion cross section, see discussion in the text. The data are results from BELLE [6].

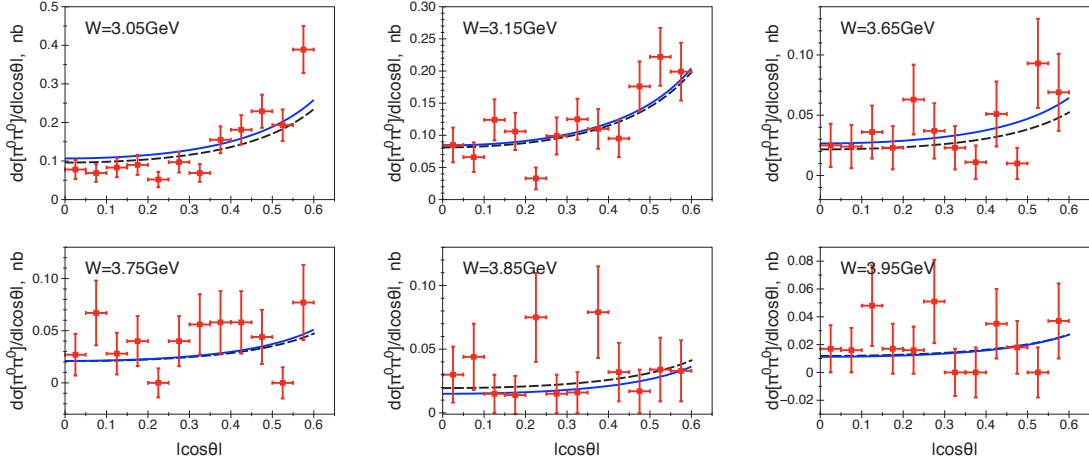


**Figure 12.** Results of the fit for the neutral pion cross section, see discussion in the text. The data are results from BELLE [7].

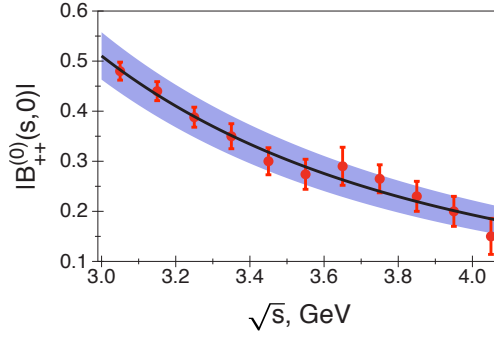


**Figure 13.** The amplitude  $B_{++}^{(0)}(s, 0)$  as a function of energy  $s$ .

where the subscripts indicate the corresponding contribution in the previous line. Hence we observe that the interference (linear in  $B_{++}^{(0)}$ ) contribution provides quite sizable effect of order 30% and therefore can not be ignored. The similar result for the neutral channel yields

$$\frac{d\sigma^{\pi^0\pi^0}}{d\cos\theta} = 0.440|B_{++}^{(0)}|^2 + 0.004 = 0.096 + 0.004 = 0.01. \quad (5.17)$$

In this case the interference term depends only from the small  $B_{+-}^{(0)}$  and therefore its effect is negligible. Then we can conclude that the sizable deviation from the value 1/2 for the cross section ratio (5.9) can be only obtained due to the effect from the linear with respect to  $B_{++}^{(0)}$  contribution.

Performing the simple power fit of results in Table 2 we obtain

$$B_{++}^{(0)}(s, 0) = \left(\frac{s_0}{s}\right)^a, \quad \text{with } s_0 = 6.0 \pm 0.3, \quad a = 1.7 \pm 0.15. \quad (5.18)$$

This result is shown in Fig.13. From the analysis carried out in Sec.3 we expect that

$$B_{++}^{(0)}(s, 0) \stackrel{s \rightarrow \infty}{\sim} \frac{\Lambda^2}{s} \left( \frac{\Lambda}{\sqrt{s}} + \alpha \frac{\Lambda^2}{s} \right), \quad (5.19)$$

where the first term  $\sim s^{-3/2}$  is related to the specific soft-overlap configuration with the soft quark and which does not overlap with any hard contribution (see discussion of the T-products (3.50) and (3.51) in Sec.3). Comparing the obtained value of the exponent  $a$  in Eq.(5.18) with this asymptotic prediction we observe a rather good agreement. If such scenario is correct then, probably, the large obtained value of  $s_0$  in Eq.Bppfit can be explained by the effect of the chiral symmetry breaking because the correction of order  $1/\sqrt{s}$  is described by the large chiral enhanced twist-3 DA.

Using the model (5.18) for  $B_{++}^{(0)}(s, 0)$  we compute the total cross sections and their ratio. The comparison of the obtained cross sections with the data is shown in Fig.14. Remind that we used the obtained values of  $B_{++}^{(0)}(s, 0)$  in order to describe the neutral pion cross section. The ratio of the total cross sections  $\sigma_{tot}^{\pi^0\pi^0}/\sigma_{tot}^{\pi^+\pi^-}$  as a function of energy is shown in Fig.15. In Fig.14 it is seen that computed  $\sigma_{tot}^{\pi^0\pi^0}$  a little bit underestimates the experimental values of the cross section and as a result the obtained ratio (solid line in

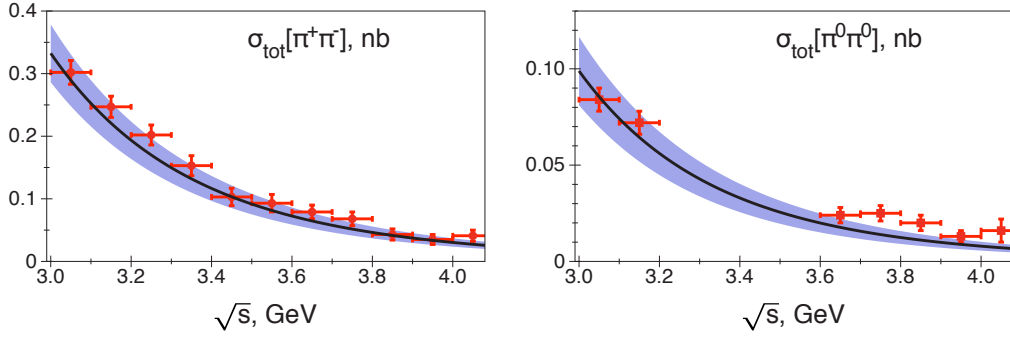


**Figure 14.** The total cross sections as a functions of energy.

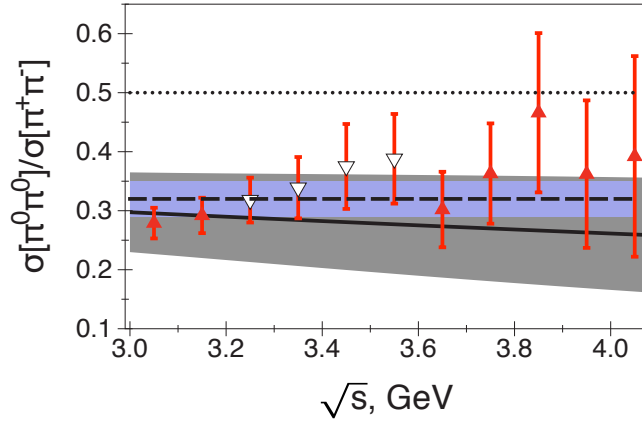


**Figure 15.** The ratio of the cross sections  $\sigma_{tot}^{\pi^0\pi^0}/\sigma_{tot}^{\pi^+\pi^-}$  as a function of the energy. The data are taken from Ref.[7]. The dashed line shows the experimental fit with  $1\sigma$  error bands. The solid line shows the computed ratio with the  $1\sigma$  error bands.

Fig.15) decreases slightly when the energy  $W$  is rising. The gray bounds around the solid line shows  $1\sigma$  bands associated with the errors of the parameters  $s_0$  and  $a$  in Eq.(5.18). The simple fit of the experimental data yields  $R = 0.32 \pm 0.03$  [7].<sup>7</sup> In Fig.15 this result is shown by dashed line with  $1\sigma$  error bands. Our estimate is consistent with the experimental fit within the error bars.

## 5.2 Analysis of BELLE data using the CZ-model of pion DA

Using the CZ-model (2.36) and fixing the small value of the renormalization scale  $\mu_R = 1.3\text{GeV}$  one obtains the larger contribution for the leading twist part. In that case the numerical value for the differential cross sections at  $W = 3.05\text{GeV}$  and  $\cos\theta = 0.05$  (c.f.

<sup>7</sup>The results in the  $W$  region  $3.3 - 3.6$  GeV (plotted with open triangles) are not used for the fit [7].



with the corresponding Eqs.(5.10)-(5.13) for the BA-model)

$$\left(\frac{d\sigma^{\pi^+\pi^-}}{d\cos\theta}\right)_{\text{LT}} = 0.18, \quad \left(\frac{d\sigma^{\pi^+\pi^-}}{d\cos\theta}\right)_{\text{exp}} = 0.312 \pm 0.039, \quad (5.20)$$

$$\left(\frac{d\sigma^{\pi^0\pi^0}}{d\cos\theta}\right)_{\text{LT}} = 0.009, \quad \left(\frac{d\sigma^{\pi^0\pi^0}}{d\cos\theta}\right)_{\text{exp}} = 0.078 \pm 0.025, \quad (5.21)$$

$$\frac{d\sigma^{\pi^+\pi^-}}{d\cos\theta} = 0.88|B_{++}^{(0)}|^2 + 0.88|B_{+-}^{(0)}|^2 - 0.65B_{++}^{(0)} - 0.45B_{+-}^{(0)} + 0.18. \quad (5.22)$$

$$\frac{d\sigma^{\pi^0\pi^0}}{d\cos\theta} = 0.44|B_{++}^{(0)}|^2 + 0.44|B_{+-}^{(0)}|^2 - 0.16B_{+-}^{(0)} + 0.014. \quad (5.23)$$

In this case the two-parameter fit is better then for the previous case: the obtained error bars are smaller. The results for the differential cross sections are shown in Fig.16 and the numerical values of the amplitudes are summarized in Table 3. We observe that in this case the solution is given by large  $B_{+-}^{(0)}$  and relatively small  $B_{++}^{(0)}$ . The coefficient of the linear contribution  $\lambda_{+-}$  defined in (5.7) is quite large and therefore the angular separation can be done easier that explains the better results of the two-parameter fit. In Fig.16 we show only the plots which describe the both pion production channels. The power fit of the amplitudes yields

$$B_{++}^{(0)}(s, 0) = \left(\frac{s_0}{s}\right)^a, \quad \text{with } s_0 = 5.8 \pm 1\text{GeV}^2, \quad a = 3.4 \pm 1.2, \quad (5.24)$$

$$B_{+-}^{(0)}(s, 0) = -\left(\frac{s_1}{s}\right)^b, \quad \text{with } s_1 = 6.1 \pm 0.5\text{GeV}^2, \quad b = 1.2 \pm 0.15. \quad (5.25)$$

The results with the  $1\sigma$  error bands are shown in Fig.17. One can observe that the absolute

**Table 3.** Results for the amplitudes  $B_{\pm\pm}^{(0)}(s, 0)$  obtained from the two-parameter fit of the BELLE data [6, 7] for pion production with CZ-model of pion DA (dof=16).

$W, \text{ GeV}$	3.05	3.15	3.65	3.75	3.85	3.95
$B_{++}^{(0)}(s, 0)$	$-0.20 \pm 0.03$	$-0.15 \pm 0.03$	$-0.09 \pm 0.05$	$-0.06 \pm 0.04$	$-0.02 \pm 0.04$	$-0.017 \pm 0.046$
$B_{+-}^{(0)}(s, 0)$	$0.59 \pm 0.03$	$0.59 \pm 0.03$	$0.36 \pm 0.04$	$0.37 \pm 0.04$	$0.37 \pm 0.03$	$0.31 \pm 0.04$
$\chi^2/\text{dof}$	2.7	2.2	0.94	1.3	0.7	0.60

value of  $B_{++}^{(0)}$  is smaller comparing to  $B_{+-}^{(0)}$  and stronger suppressed with energy. The power behavior of the dominant amplitude  $B_{+-}^{(0)}$  is again close to the SCET asymptotic prediction  $\sim 1/s^{3/2}$  as in Eq.(5.19). The one-parameter model with  $B_{++}^{(0)} \simeq 0$  in this case shows much worse description indicating that  $B_{++}^{(0)}$  can not be neglected for the all values of energy. The total cross sections and their ratio are shown in Fig.18 and Fig.19. We used the same notation as before and the error bands in the all figures has the same meaning as in Fig.14 and Fig.15, respectively.

In case of CZ-model one also needs to take into account the large numerical effect provided by the amplitudes  $B_{+\pm}^{(0)}$  including the linear contributions. Substituting the numerical values for the amplitude in Eqs. (5.22) and (5.23) we obtain (remind that we fixed  $W = 3.05\text{GeV}$  and  $\cos\theta = 0.05$ )

$$\frac{d\sigma^{\pi^+\pi^-}}{d\cos\theta} = 0.035_{B_{++}^2} + 0.3_{B_{+-}^2} + 0.13_{B_{++}} - 0.26_{B_{+-}} + 0.18 = 0.38, \quad (5.26)$$

$$\frac{d\sigma^{\pi^0\pi^0}}{d\cos\theta} = 0.018_{B_{++}^2} + 0.15_{B_{+-}^2} - 0.09_{B_{+-}} + 0.014 = 0.09. \quad (5.27)$$

Here the subscripts again show the numerical contribution of the appropriate quadratical or linear terms in Eq's.(5.22) and (5.23). Numerical results in (5.26) and (5.27) demonstrate that the final value is in the nontrivial sum of the all terms and contribution from the amplitudes  $B_{+\pm}^{(0)}$  is again significant for description of the both cross sections.

The fact that the two-parameter fit is better for CZ-model can not be considered as a supporting argument for this model against the other ones. We find that it is very difficult to make any definite conclusion about the preferred models for the pion DA without an additional information. More experimental data can be obtained in from electron-positron collisions measuring the cross section  $e^+e^- \rightarrow e^+e^-\pi\pi$  with unpolarized electron beams and reaction  $\gamma\gamma \rightarrow \pi\pi$  as the hadronic subprocess. The cross section for such process is described by the two contributions, see the details in Ref.[1]. Schematically the expression for the cross section reads

$$d\sigma^{e^+e^- \rightarrow e^+e^-\pi\pi} = \left\{ A \frac{1}{2} \left( \sigma_{\parallel}^{\gamma\gamma \rightarrow \pi\pi} + \sigma_{\perp}^{\gamma\gamma \rightarrow \pi\pi} \right) + B \left( \sigma_{\parallel}^{\gamma\gamma \rightarrow \pi\pi} - \sigma_{\perp}^{\gamma\gamma \rightarrow \pi\pi} \right) \cos 2\varphi \right\} \frac{d^3p'_1}{E_1} \frac{d^3p'_2}{E_1}, \quad (5.28)$$

where the  $\sigma_{\parallel,\perp}^{\gamma\gamma \rightarrow \pi\pi}$  denotes cross sections for the scattering of photons with the parallel ( $\sigma_{\parallel}$ ) and orthogonal ( $\sigma_{\perp}$ ) linear polarizations. Here the coefficients  $A$  and  $B$  denote the known functions of kinematical variables and can be found in Ref.[1]. The azimuth angle  $\varphi$  is defined as the angle between the electron scattering planes in the colliding electron c.m.s. The  $E_i$  and  $p'_i$  describe the scattered electron energies and momenta. In the present work we investigated the first combination of the cross sections which is proportional to the sum of the helicity amplitudes:

$$\sigma_{\parallel}^{\gamma\gamma \rightarrow \pi\pi} + \sigma_{\perp}^{\gamma\gamma \rightarrow \pi\pi} \sim |T_{++}^{\gamma\gamma \rightarrow \pi\pi}|^2 + |T_{+-}^{\gamma\gamma \rightarrow \pi\pi}|^2. \quad (5.29)$$

Using the angular dependence given by the factor  $\cos 2\varphi$  one can also access the second contribution which is sensitive to the difference of the cross sections in Eq.(5.28). This combination is proportional only to the one helicity amplitude

$$\sigma_{\parallel}^{\gamma\gamma \rightarrow \pi\pi} - \sigma_{\perp}^{\gamma\gamma \rightarrow \pi\pi} \sim |T_{++}^{\gamma\gamma \rightarrow \pi\pi}|^2. \quad (5.30)$$

Therefore using this data one can perform the much better separation of the helicity amplitudes and extraction of the unknown soft-overlap form factors  $B^{(0)\pm}(s, 0)$ . Moreover,

the predictions of the different models are sensitive to the value  $|T_{++}^{\gamma\gamma\rightarrow\pi\pi}|$ . For instance, the calculations within the handbag model in Ref.[17] provide  $T_{++}^{\gamma\gamma\rightarrow\pi\pi} \simeq 0$ .

In presented consideration the value of the amplitudes  $B^{(0)\pm}(s, 0)$  depends on the model of the pion DA used for the fit. In case of BA-model we obtained that  $|T_{++}^{\gamma\gamma\rightarrow\pi\pi}| \gg |T_{+-}^{\gamma\gamma\rightarrow\pi\pi}|$  and contrawise for the CZ-model. The predictions for the combination  $\sigma_{\parallel} - \sigma_{\perp}$  at  $W = 3.05\text{GeV}$  and two different models of pion DA are shown in Fig.20. In order to draw these plots we used the values of the amplitude  $B_{++}^{(0)}(s, 0)$  obtained in Tables 2 and 3. The shaded areas show  $1\sigma$  error bands which appear due to the uncertainties in the determination of  $B_{++}^{(0)}(s, 0)$ . Unfortunately the difference between the two predictions is not large and does not allow one to make very clear statement about the preferred scenario. Nevertheless we expect that the more data for the combination of the cross sections  $\sigma_{\parallel}^{\gamma\gamma\rightarrow\pi\pi} - \sigma_{\perp}^{\gamma\gamma\rightarrow\pi\pi}$  can be very helpful in order to understand the reaction mechanism of the hard exclusive hadron pair production at intermediate values of the energy and momentum transfer.

## 6 Discussion

In conclusion, we discussed the calculation of the subleading power corrections to the amplitude of the process  $\gamma\gamma \rightarrow \pi\pi$  in the region where all Mandelstam variables are large  $s \sim -t \sim -u \gg \Lambda^2$  (large angle scattering). The leading power behavior of the corresponding amplitude is described by the hard scattering mechanism suggested in Ref.[2]. The power corrections to this result can be presented as a sum of the hard and soft-overlap contributions. We try to develop a systematic approach for description of such configurations using the SCET framework. In this approach the soft-overlap contribution can be defined as a matrix elements of the suitable SCET-I operators. We carried out the analysis of the relevant SCET-I operators which one needs in order to describe  $1/Q$  and  $1/Q^2$  corrections to the leading power approximation. We demonstrated that these SCET-I operators can mix in SCET-II with the collinear operators which describe the hard subleading contributions. Such mixing corresponds to the overlap of the collinear and soft domains and leads to the appearance of the end-point singularities in the convolution integrals. Therefore in order to factorize the hard and soft contributions one has to define a specific regularization in order to treat the rapidity divergencies. In a certain situations such a complicated scheme can be avoided if one uses the so-called physical subtraction scheme. We used this method in the present work.

We obtained that the soft-overlap contribution is described by many different SCET-I operators. These operators can be associated with different soft-overlap configurations. To the leading order accuracy in the hard  $\alpha_s$  only the soft-overlap between the outgoing two-pion states is relevant. Nevertheless there are many suitable SCET-I operators which are relevant for description of this configuration.

Among them there is an operator which plays the special role. This operator is built from the two quark and one gluon hard-collinear fields and appears to be the leading order operator according to the SCET-I counting rules. The feature of this operator is that at large energy limit its matrix element describes the soft contributions suppressed as  $1/\sqrt{s}$

and  $1/s$  comparing to the leading power approximation. All other SCET-I operators describe the soft-overlap contributions suppressed as  $1/s$ . We observed that the soft-overlap configuration associated with the  $1/\sqrt{s}$  behavior does not overlap with any hard contribution, i.e one can not construct any collinear operator (assuming that only the massless quarks describe the hard subprocess) which can provide the similar scaling behavior.

The hard contributions are described by the matrix elements of the pure collinear operators. All such subleading contributions provide the relative correction of order  $1/s$ .

As we mentioned before there are many SCET-I operators which in SCET-II can mix with the collinear operators associated with the hard configuration. In this work we took into account only the specific collinear operators which can provide the largest numerical corrections. Such terms are described by the twist-3 two-particle collinear operators and often referred as chiral enhanced corrections.

We obtained that the corresponding hard contributions in the amplitudes have the end-point singularities. In order to be consistent we considered the SCET-I operator which can overlap with this hard contribution. We demonstrated that the sum of the soft and hard contributions can be reorganized using the physical subtraction scheme in a such way that the resulting expression for the amplitude is finite.

The fact that in the leading-order in  $\alpha_s$  we obtained the soft contribution describing the soft-overlap of the two-pion states allows us to compute the angular dependence of the amplitudes in a model independent way. Therefore our final expression for the subleading power corrections depends only from the two unknown form factors  $B_{+\pm}^0(s, 0)$  which are some functions of the energy  $s$ . These two parameters can be interpreted as a soft-overlap contributions to the helicity amplitudes describing the two-pion production. In the kinematical region  $\sqrt{s} = 3 - 4\text{GeV}$  the energy dependence of these functions can not be computed because the hard-collinear scale is still relatively small.

In order to fix these nonperturbative functions we carried out the analysis of the differential cross sections in the region  $\sqrt{s} = 3 - 4\text{GeV}$  and  $|\cos\theta| < 0.6$ . The amplitudes in this analysis are given by the sum of the leading and subleading power corrections. We obtain that to a very good accuracy the angular behavior of the cross section for the production of charged pions is proportional to the  $\sin^{-4}\theta$  that is in the good agreement with the existing data. We also obtained that existing data can be reasonably described by the suitable choice of the form factors  $B_{+\pm}^{(0)}(s, 0)$ .

The results for the functions  $B_{+\pm}^{(0)}(s, 0)$  are sensitive to the models of pion distribution amplitude used in the numerical calculations. For the CZ-model the best fit is obtained if  $|B_{+-}^{(0)}(s, 0)| \gg |B_{++}^{(0)}(s, 0)|$ . For the other models of pion DA the angular separation of the amplitudes  $B_{+\pm}^{(0)}(s, 0)$  can not be done with a good precision but the fit allowed us to obtain the qualitative estimate  $|B_{++}^{(0)}(s, 0)| \gg |B_{+-}^{(0)}(s, 0)|$ . Following this observation we suggested the model with  $B_{+-}^{(0)}(s, 0) = 0$  and found that the data can be rather well described in this case.

We obtained a reasonable description of the ratio of the cross sections  $R = d\sigma^{\pi^0\pi^0}/d\sigma^{\pi^+\pi^-}$  for the all models of pion distribution amplitude. In all cases we observed that the interference of the leading and subleading power corrections provides an important numerical

contribution. As a result this provides a possibility to obtain the ratio  $R < 1/2$  which is consistent with the experimental data.

The energy behavior of the extracted functions  $B_{+\pm}^{(0)}(s, 0)$  is consistent within the error bars with the asymptotic behavior  $s^{-3/2}$  expected from SCET estimates. Might be this can be explained by the domination of the specific soft contribution described by the leading SCET-I operator.

Unfortunately, our analysis does not allow us to discriminate between the scenarios with the different model of the pion distribution amplitude. For that we need an additional experimental information. More accurate data, especially for larger values of energy will be very helpful but one has to remember that our description is also restricted only by the leading-order accuracy. The calculations beyond the leading-order will unavoidably involve into the consideration the new soft-overlap configurations which describe the overlap of the real photon with pion(s) and this makes the systematic consideration more complicate and reduces the predictive power of the theoretical description.

The other chance to improve the analysis is to have an additional observable which is sensitive to a different combination of the helicity amplitudes. Such a cross section can be accessed in the exclusive process  $e^+e^- \rightarrow e^+e^-\pi\pi$  if one measures the cross section as a function of the angle between the electron scattering planes in the colliding electron c.m.s., see e.g. Ref.[1]. In this case one can access the combination  $\sigma_{\parallel}^{\gamma\gamma \rightarrow \pi\pi} - \sigma_{\perp}^{\gamma\gamma \rightarrow \pi\pi} \sim |T_{++}^{\gamma\gamma \rightarrow \pi\pi}|^2$ , where the  $\sigma_{\parallel, \perp}^{\gamma\gamma \rightarrow \pi\pi}$  denotes cross sections for the scattering of photons with parallel ( $\sigma_{\parallel}$ ) and orthogonal ( $\sigma_{\perp}$ ) linear polarizations. This observable is sensitive only to the amplitude  $B_{++}^{(0)}(s, 0)$  and therefore it allows one to improve the extraction of the amplitudes  $B_{+\pm}^{(0)}(s, 0)$  and to understand better the production mechanism in the two-photon annihilation. We suggest to consider the possibility of such measurements in BES-III experiment which has high luminosity beam and one can perform the measurements in the kinematical region where the energy and momentum transfer are sufficiently large.

## A Higher twist pion distribution amplitudes

In this Appendix we provide a list of higher twist pion DAs up to twist-4. More detailed discussion can be found in Ref.[43]. Below we present the standard QCD formulation. In order to obtain the SCET formulation one has to split the quark fields into large  $\xi_n$  and small  $\eta_n$  components and use the equation of motion in order to eliminate the field  $\eta_n$ . The discussion of the collinear matrix elements in SCET in the hybrid approach can be found in Ref.[39].

In SCET the twist-3 DAs describe the matrix element to the collinear operator  $O_c^{(6)}$  in Eq.(3.19). In the usual QCD formulation there are three twist-3 collinear operators. Two of them are 2-particle operators and their light-cone matrix elements are defined as

$$\langle p' | \bar{q}(\lambda_1 \bar{n}) W_n(\lambda_1 \bar{n}) i\gamma_5 W_n^\dagger(\lambda_1 \bar{n}) q(\lambda_2 \bar{n}) | 0 \rangle = f_\pi \mu_\pi \int_0^1 du e^{iu\lambda_1 p'_- + i\bar{u}\lambda_2 p'_-} \phi_p(u), \quad (\text{A.1})$$

$$\langle p' | \bar{q}(\lambda_1 \bar{n}) W_n(\lambda_1 \bar{n}) \sigma^{\alpha\beta} \gamma_5 W_n^\dagger(\lambda_2 \bar{n}) q(\lambda_2 \bar{n}) | 0 \rangle = i f_\pi \mu_\pi \left( p^\alpha z^\beta - p^\beta z^\alpha \right) \quad (\text{A.2})$$

$$\int_0^1 du e^{iu\lambda_1 p'_- + i\bar{u}\lambda_2 p'_-} \frac{\phi_\sigma(u)}{6}, \quad (\text{A.3})$$

with  $z^\alpha = (\lambda_1 - \lambda_2) \bar{n}^\alpha$ ,  $p'_- \equiv (p' \cdot \bar{n})$  and

$$\mu_\pi = \frac{m_\pi^2}{m_u + m_d}, \quad p' \simeq p'_- \frac{\bar{n}}{2}. \quad (\text{A.4})$$

For the sum of the quark masses we use following estimate

$$(m_u + m_d)(2\text{GeV}) = 8.5\text{MeV}. \quad (\text{A.5})$$

There is only one twist-3 three-particle operator and its matrix element defines the three-particle DA  $\phi_{3\pi}(\alpha_i)$

$$\langle \pi^+(p') | \bar{u}(\lambda \bar{n}) \sigma^{\bar{n}\alpha\perp} \gamma_5 g G_{\bar{n}\alpha\perp}(v\lambda \bar{n}) d(-\lambda \bar{n}) | 0 \rangle = i f_{3\pi} p_-'^2 2 \int \mathcal{D}\alpha_i e^{i\lambda p'_-(\alpha_u - \alpha_d + v\alpha_g)} \phi_{3\pi}(\alpha_i), \quad (\text{A.6})$$

Here  $\mathcal{D}\alpha_i = d\alpha_u d\alpha_d d\alpha_g \delta(\alpha_u + \alpha_d + \alpha_g - 1)$ ,  $G_{\bar{n}\alpha\perp} = G_{\mu\alpha\perp} \bar{n}^\mu$ . Using QCD equations of motion one can show ( see details in Refs.[43, 48]) that 2-particles DAs  $\phi_{p,\sigma}$  can be presented as

$$\phi_p(u) = 1 + R V_p(u, \alpha_i) * \phi_{3\pi}(\alpha_i), \quad (\text{A.7})$$

$$\phi_\sigma(u) = 6u\bar{u} + R V_\sigma(u, \alpha_i) * \phi_{3\pi}(\alpha_i), \quad (\text{A.8})$$

where  $V_{p,\sigma}$  denotes a certain dimensionless kernel, the asterisks denote the convolution integrals with respect to the fractions  $\alpha_i$  and  $R = f_{3\pi}/f_\pi \mu_\pi \simeq 0.014$  [43, 48]. One can assume that corrections associated with the admixture  $\phi_{3\pi}$  in Eqs.(A.7) and (A.8) are relatively small because the factor  $R$  is numerically small comparing to the constant  $\mu_\pi$  defined in Eq.(A.4). Therefore if one neglects the 3-particle contributions with  $\phi_{3\pi}$  in Eqs. (A.7) and (A.8) one finds

$$\phi_p(u) \simeq 1, \quad \phi_\sigma(u) \simeq 6u\bar{u}. \quad (\text{A.9})$$

In QCD formalism there are four three-particle DA's of twist four. They are defined as (below we do not write the collinear Wilson lines  $W_n$  for simplicity)

$$\langle \pi^+(p') | \bar{u}(\lambda \bar{n}) \gamma_\perp^\alpha \gamma_5 g G_{\alpha\perp \bar{n}}(v\lambda \bar{n}) d(-\lambda \bar{n}) | 0 \rangle = 2f_\pi m_\pi^2 p'_- A_\perp(v, \lambda p'_-), \quad (\text{A.10})$$

$$\langle \pi^+(p') | \bar{u}(\lambda \bar{n}) \gamma_\perp^\alpha g \tilde{G}_{\alpha\perp \bar{n}}(v\lambda \bar{n}) d(-\lambda \bar{n}) | 0 \rangle = 2f_\pi m_\pi^2 p'_- V_\perp(v, \lambda p'_-), \quad (\text{A.11})$$

$$\langle \pi^+(p') | \bar{u}(\lambda \bar{n}) \not{n} \gamma_5 g G_{\bar{n}n}(v\lambda \bar{n}) d(-\lambda \bar{n}) | 0 \rangle = f_\pi m_\pi^2 p'_- A_\parallel(v, \lambda p'_-), \quad (\text{A.12})$$

$$\langle \pi^+(p') | \bar{u}(\lambda \bar{n}) \not{n} g \tilde{G}_{\bar{n}n}(v\lambda \bar{n}) d(-\lambda \bar{n}) | 0 \rangle = f_\pi m_\pi^2 p'_- V_\parallel(v, \lambda p'_-), \quad (\text{A.13})$$

with the

$$\{V_i, A_i\}(v, \lambda p'_-) = \int \mathcal{D}\alpha_i e^{i\lambda p'_-(\alpha_u - \alpha_d + v\alpha_g)} \{V_i, A_i\}(\alpha_i). \quad (\text{A.14})$$

and we used

$$\tilde{G}_{\alpha\beta} = \frac{1}{2} \varepsilon_{\alpha\beta\mu\nu} G^{\mu\nu}. \quad (\text{A.15})$$

Here we will not discuss the structure of these DAs because we neglect these contributions in our calculations.

In the SCET framework there are also two-particle collinear operators which we do not include in the list in Eq.(3.19) because they are not independent. Let us now discuss the correspondence of the two-particle twist-3 operators with the two-particle operators appearing in SCET. Consider first the pseudoscalar operator as in Eq. (A.1)

$$O_p = \bar{q}(y)W_n(y)i\gamma_5 W_n^\dagger(x)q(x). \quad (\text{A.16})$$

Writing the QCD quark fields as sum of large  $\xi_n$  and small  $\eta_n$  fields in position space and eliminating  $\eta_n$  by equation of motion one finds, see e.g. Ref.[23]

$$q = \xi_n + \eta_n = \xi_n - \frac{\not{n}}{2} (i\bar{n}D + i0)^{-1} i\not{D}_\perp \xi_n, \quad (\text{A.17})$$

$$\bar{q} = \bar{\xi}_n - \bar{\xi}_n i\overleftarrow{\not{D}}_\perp \left( i\bar{n}\overleftarrow{D} - i0 \right)^{-1} \frac{\not{n}}{2} \quad (\text{A.18})$$

In what follow we skip the subscript  $n$  and assume that

$$\xi_n \equiv \xi, \quad \not{n}\xi = 0, \quad W_n \equiv W. \quad (\text{A.19})$$

Substituting expressions (A.17) and (A.18) into Eq.(A.16) we obtain

$$O_p = -\bar{\xi}W(y_+)i\gamma_5 \frac{\not{n}}{2} \left[ W^\dagger (i\bar{n}D)^{-1} i\not{D}_\perp \xi \right] (x_+) - \left[ \bar{\xi} i\overleftarrow{\not{D}}_\perp \left( i\bar{n}\overleftarrow{D} \right)^{-1} \frac{\not{n}}{2} W \right] (y_+) i\gamma_5 W^\dagger \xi(x_+). \quad (\text{A.20})$$

where we use

$$y_+ = (yn)\frac{\bar{n}}{2}, \quad x_+ = (xn)\frac{\bar{n}}{2}, \quad (\text{A.21})$$

and

$$\bar{\xi}W(y_+) \equiv \bar{\xi}_n(y_+)W_n(y_+). \quad (\text{A.22})$$

Let us rewrite the obtained expression in terms of gauge invariant combinations  $\chi$  as in Eq.(3.6). In order to do this we use simple identity

$$W^\dagger (i\bar{n}D + i0)^{-1} iD_\mu \xi(x_+) = (i\bar{n}\partial)^{-1} W^\dagger iD_\mu \xi(x_+) = (i\bar{n}\partial)^{-1} W^\dagger (i\partial_\mu + gA_\mu) \xi(x_+) \quad (\text{A.23})$$

$$= (i\bar{n}\partial)^{-1} W^\dagger (gA_\mu) \xi(x_+) + (i\bar{n}\partial)^{-1} i\partial_\mu W^\dagger \xi(x_+) - (i\bar{n}\partial)^{-1} \left[ i\partial_\mu W^\dagger \right] \xi(x_+) \quad (\text{A.24})$$

$$= (i\bar{n}\partial)^{-1} i\partial_\mu \left[ W^\dagger \xi \right] (x_+) - (i\bar{n}\partial)^{-1} \left[ W^\dagger \left( i\overleftarrow{\partial}_\mu - gA_\mu \right) \right] \xi(x_+) \quad (\text{A.25})$$

$$= (i\bar{n}\partial)^{-1} i\partial_\mu \left[ W^\dagger \xi \right] (x_+) - (i\bar{n}\partial)^{-1} \left[ W^\dagger i\overleftarrow{D}_\mu W \right] W^\dagger \xi(x_+). \quad (\text{A.26})$$

Therefore we obtain

$$W^\dagger (i\bar{n}D + i0)^{-1} iD_\mu \xi(x_+) = (i\bar{n}\partial)^{-1} i\partial_\mu \chi(x_+) - (i\bar{n}\partial)^{-1} \mathcal{A}_\mu(x_+) \chi(x_+). \quad (\text{A.27})$$

The similar reorganization yields

$$\bar{\xi} i\overleftarrow{D}_\mu \left( i\bar{n}\overleftarrow{D} \right)^{-1} W(y_+) = \bar{\chi}(y_+) i\overleftarrow{\partial}_\mu \left( i\bar{n}\overleftarrow{\partial} \right)^{-1} - \bar{\chi}(y_+) \mathcal{A}_\mu(x_+) \left( i\bar{n}\overleftarrow{\partial} \right)^{-1}. \quad (\text{A.28})$$

Using the expressions (A.27) and (A.28) in Eq.(A.20) we find

$$O_p = -\bar{\chi}(y_+) i\gamma_5 \frac{\not{n}}{2} \frac{i\not{\partial}_\perp}{i\bar{n}\partial} \chi(x_+) - \bar{\chi}(y_+) \left( i\bar{n} \overleftarrow{\partial} \right)^{-1} i \overleftarrow{\not{\partial}}_\perp \frac{\not{n}}{2} i\gamma_5 \chi(x_+) + \dots, \quad (\text{A.29})$$

where dots denotes the three particle contributions with the gluon fields  $\mathcal{A}_\mu$ . These three-particle contributions provide the terms proportional to the small factor  $R$  in Eq.(A.7). Substituting the SCET expression (A.29) into Eq.(A.1) and neglecting the 3-particle terms we obtain

$$\begin{aligned} & -\langle p' | \bar{\chi}(y_+) i\gamma_5 \frac{\not{n}}{2} i\not{\partial}_\perp (i\bar{n}\partial)^{-1} \chi(x_+) + \bar{\chi}(y_+) \left( i\bar{n} \overleftarrow{\partial} \right)^{-1} i \overleftarrow{\not{\partial}}_\perp \frac{\not{n}}{2} i\gamma_5 \chi(x_+) | 0 \rangle \\ & = f_\pi \mu_\pi \int_0^1 du e^{iu} p'_- y_+/2 + i\bar{u} p'_- x_+/2 \phi_p(u), \end{aligned} \quad (\text{A.30})$$

Let us define the Fourier transformation as

$$\text{FT} \equiv \left( \frac{p'_-}{2} \right)^2 \int \frac{dy_+}{2\pi} e^{-iy_+ p'_- t_1/2} \int \frac{dx_+}{2\pi} e^{-ix_+ p'_- t_2/2}. \quad (\text{A.31})$$

Then

$$\text{FT} \int_0^1 du e^{iu} p'_- y_+/2 + i\bar{u} p'_- x_+/2 \phi_p(u) = \delta(1 - t_1 - t_2) \phi_p(t_1) \equiv \phi_p(t). \quad (\text{A.32})$$

On the other hand the FT of the expression in lhs of Eq.(A.30) can be rewritten as

$$\text{FT} \langle p' | \bar{\chi}(y_+) i\gamma_5 \frac{\not{n}}{2} i\not{\partial}_\perp (i\bar{n}\partial)^{-1} \chi(x_+) | 0 \rangle = (-i) \int_{-\infty}^0 ds \text{FT} \langle p' | \bar{\chi}(y_+) i\gamma_5 \frac{\not{n}}{2} i\not{\partial}_\perp \chi(x_+ + s\bar{n}) | 0 \rangle \quad (\text{A.33})$$

$$= (-i) \int_{-\infty}^0 ds \int \frac{dy_+}{2\pi} e^{-iy_+ p'_- t_1/2} \int \frac{dx_+}{2\pi} e^{-i(x_+ - 2s)p'_- t_2/2} \langle k | \bar{\chi}(y_+) i\gamma_5 \frac{\not{n}}{2} i\not{\partial}_\perp \chi(x_+) | 0 \rangle \quad (\text{A.34})$$

$$= \text{FT}(-i) \int_{-\infty}^0 ds e^{\varepsilon s + i s p'_- t_2} \langle p' | \bar{\chi}(y_+) i\gamma_5 \frac{\not{n}}{2} i\not{\partial}_\perp \chi(x_+) | 0 \rangle \quad (\text{A.35})$$

$$= -\frac{1}{k_-} \frac{1}{1-t} \text{FT} \langle p' | \bar{\chi}(y_+) i\gamma_5 \frac{\not{n}}{2} i\not{\partial}_\perp \chi(x_+) | 0 \rangle. \quad (\text{A.36})$$

The similar calculations for the second term in Eq.(A.30) yield

$$\text{FT} \langle p' | \bar{\chi}(y_+) \left( i\bar{n} \overleftarrow{\partial} \right)^{-1} i \overleftarrow{\not{\partial}}_\perp \frac{\not{n}}{2} i\gamma_5 \chi(x_+) | 0 \rangle = -\frac{1}{p'_-} \frac{1}{t} \text{FT} \langle p' | (\bar{\chi}(y_+) i\not{\partial}_\perp) \frac{\not{n}}{2} i\gamma_5 \chi(x_+) | 0 \rangle \quad (\text{A.37})$$

$$= \frac{1}{p'_-} \frac{1}{t} \text{FT} \langle p' | \bar{\chi}(y_+) \frac{\not{n}}{2} i\gamma_5 i\not{\partial}_\perp \chi(x_+) | 0 \rangle. \quad (\text{A.38})$$

Therefore, substituting in (A.30) and using that  $\phi_p(t) \simeq 1$  we obtain

$$\text{FT} \langle p' | \bar{\chi}(y_+) \frac{\not{n}}{2} i\gamma_5 i\not{\partial}_\perp \chi(x_+) | 0 \rangle \simeq p'_- f_\pi \mu_\pi t \bar{t}. \quad (\text{A.39})$$

From this consideration one sees that the matrix element of the two-particle SCET operator is not independent and can be presented in the form similar to Eq.(A.7).



## Acknowledgments

This work was supported by the Helmholtz Institute Mainz. The author is grateful to M. Vanderhaeghen, M. Distler and L. Tiator for many useful discussions and to S. Eydelman and H. Nakazawa for the helpful correspondence.

## References

- [1] V. M. Budnev, I. F. Ginzburg, G. V. Meledin and V. G. Serbo, Phys. Rept. **15** (1975) 181.
- [2] S. J. Brodsky and G. P. Lepage, Phys. Rev. D **24** (1981) 1808.
- [3] M. Benayoun and V. L. Chernyak, Nucl. Phys. B **329** (1990) 285.
- [4] J. Dominick *et al.* [CLEO Collaboration], Phys. Rev. D **50** (1994) 3027 [hep-ph/9403379].
- [5] A. Heister *et al.* [ALEPH Collaboration], Phys. Lett. B **569** (2003) 140.
- [6] H. Nakazawa *et al.* [BELLE Collaboration], Phys. Lett. B **615** (2005) 39 [hep-ex/0412058].
- [7] S. Uehara *et al.* [BELLE Collaboration], Phys. Rev. D **79** (2009) 052009 [arXiv:0903.3697 [hep-ex]].
- [8] J. Brodzicka *et al.* [Belle Collaboration], PTEP **2012** (2012) 04D001 [arXiv:1212.5342 [hep-ex]].
- [9] C. Vogt, hep-ph/0010040.
- [10] V. L. Chernyak, Phys. Lett. B **640** (2006) 246 [hep-ph/0605072].
- [11] V. L. Chernyak, arXiv:1212.1304 [hep-ph]; V. L. Chernyak, Chin. Phys. C **34** (2010) 822 [arXiv:0912.0623 [hep-ph]].
- [12] A. Khodjamirian, Eur. Phys. J. C **6** (1999) 477 [hep-ph/9712451].
- [13] S. S. Agaev, V. M. Braun, N. Offen and F. A. Porkert, Phys. Rev. D **86** (2012) 077504 [arXiv:1206.3968 [hep-ph]].
- [14] A. P. Bakulev, S. V. Mikhailov, A. V. Pimikov and N. G. Stefanis, Nucl. Phys. Proc. Suppl. **219-220** (2011) 133 [arXiv:1108.4344 [hep-ph]].
- [15] A. P. Bakulev, S. V. Mikhailov, A. V. Pimikov and N. G. Stefanis, Phys. Rev. D **86** (2012) 031501 [arXiv:1205.3770 [hep-ph]].
- [16] V. M. Braun, A. Khodjamirian and M. Maul, Phys. Rev. D **61** (2000) 073004 [hep-ph/9907495].
- [17] M. Diehl, P. Kroll and C. Vogt, Phys. Lett. B **532** (2002) 99 [hep-ph/0112274].
- [18] M. Diehl and P. Kroll, Phys. Lett. B **683** (2010) 165 [arXiv:0911.3317 [hep-ph]].
- [19] C. W. Bauer, S. Fleming and M. E. Luke, Phys. Rev. D **63**, 014006 (2000).
- [20] C. W. Bauer, S. Fleming, D. Pirjol and I. W. Stewart, Phys. Rev. D **63**, 114020 (2001).
- [21] C. W. Bauer and I. W. Stewart, Phys. Lett. B **516**, 134 (2001).
- [22] C. W. Bauer, D. Pirjol and I. W. Stewart, Phys. Rev. D **65**, 054022 (2002).
- [23] M. Beneke, A. P. Chapovsky, M. Diehl and T. Feldmann, Nucl. Phys. B **643**, 431 (2002).
- [24] M. Beneke and T. Feldmann, Phys. Lett. B **553**, 267 (2003).

- [25] J. Gasser, M. A. Ivanov and M. E. Sainio, Nucl. Phys. B **745** (2006) 84 [hep-ph/0602234].
- [26] G. P. Lepage and S. J. Brodsky, Phys. Lett. B **87**, 359 (1979).
- [27] V. L. Chernyak and A. R. Zhitnitsky, Phys. Rept. **112**, 173 (1984).
- [28] N. Isgur and C. H. Llewellyn Smith, Phys. Rev. Lett. **52**, 1080 (1984).
- [29] N. Isgur and C. H. Llewellyn Smith, Nucl. Phys. B **317**, 526 (1989).
- [30] N. Isgur and C. H. Llewellyn Smith, Phys. Lett. B **217**, 535 (1989).
- [31] V. A. Nesterenko and A. V. Radyushkin, Phys. Lett. B **115** (1982) 410.
- [32] A. P. Bakulev, A. V. Radyushkin and N. G. Stefanis, Phys. Rev. D **62** (2000) 113001 [hep-ph/0005085].
- [33] V. L. Chernyak and A. R. Zhitnitsky, Nucl. Phys. B **201** (1982) 492 [Erratum-ibid. B **214** (1983) 547].
- [34] A. V. Radyushkin, JINR Rapid Commun. **78** (1996) 96 [hep-ph/9907228].
- [35] G. Duplancic and B. Nizic, Phys. Rev. Lett. **97** (2006) 142003 [hep-ph/0607069].
- [36] C. W. Bauer, S. Fleming, D. Pirjol, I. Z. Rothstein and I. W. Stewart, Phys. Rev. D **66** (2002) 014017 [hep-ph/0202088].
- [37] C. W. Bauer, D. Pirjol and I. W. Stewart, Phys. Rev. D **68** (2003) 034021 [hep-ph/0303156].
- [38] M. Beneke and T. Feldmann, Nucl. Phys. B **685** (2004) 249 [hep-ph/0311335].
- [39] A. Hardmeier, E. Lunghi, D. Pirjol and D. Wyler, Nucl. Phys. B **682** (2004) 150 [hep-ph/0307171].
- [40] Y. Y. Balitsky, V. M. Braun and A. V. Kolesnichenko, Sov. J. Nucl. Phys. **48** (1988) 348 [Yad. Fiz. **48** (1988) 547]; Nucl. Phys. B **312** (1989) 509.
- [41] M. Beneke, G. Buchalla, M. Neubert and C. T. Sachrajda, Nucl. Phys. B **591** (2000) 313 [arXiv:hep-ph/0006124].
- [42] M. Beneke and T. Feldmann, Nucl. Phys. B **592** (2001) 3 [arXiv:hep-ph/0008255].
- [43] V. M. Braun and I. E. Filyanov, Z. Phys. C **48** (1990) 239 [Sov. J. Nucl. Phys. **52** (1990) 126] [Yad. Fiz. **52** (1990) 199].
- [44] N. Kivel and M. Vanderhaeghen, Phys. Rev. D **83** (2011) 093005 [arXiv:1010.5314 [hep-ph]].
- [45] J. Chay and C. Kim, Phys. Rev. D **82** (2010) 094021 [arXiv:1007.4395 [hep-ph]].
- [46] M. Beneke, Nucl. Phys. Proc. Suppl. **111** (2002) 62 [hep-ph/0202056].
- [47] R. Mertig, M. Bohm and A. Denner, Comput. Phys. Commun. **64** (1991) 345; R. Mertig and R. Scharf, Comput. Phys. Commun. **111** (1998) 265 [hep-ph/9801383]; see also web-page <http://www.feyncalc.org>
- [48] P. Ball, V. M. Braun and A. Lenz, JHEP **0605** (2006) 004 [hep-ph/0603063].

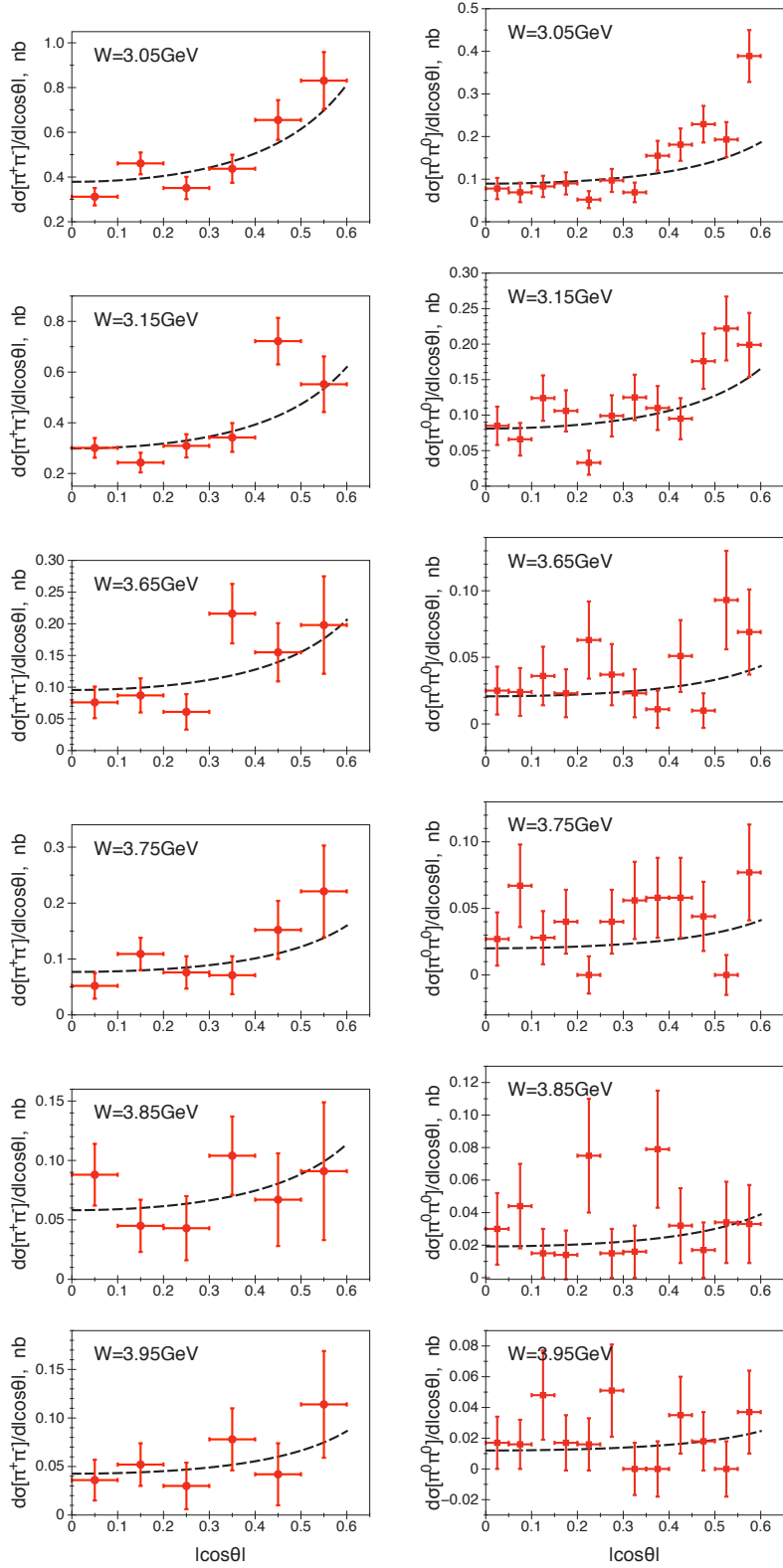


**Figure 16.** Results of the fit of BELLE data [6, 7] for the differential cross sections at different energies.

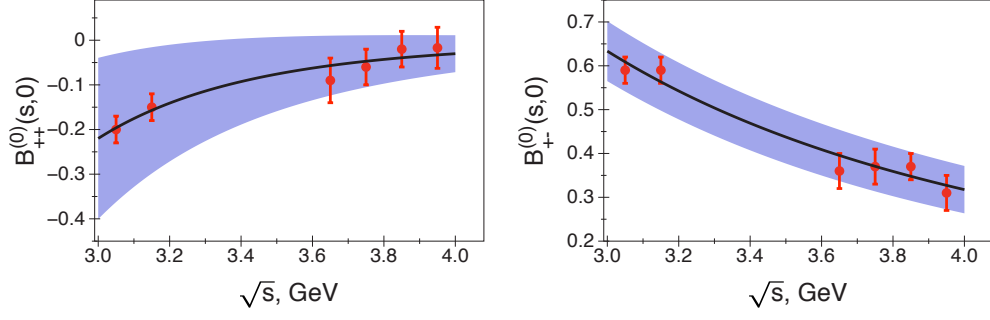


**Figure 17.** The amplitudes  $B_{++}^{(0)}(s,0)$  and  $B_{+-}^{(0)}(s,0)$  as a functions of energy obtained from the fit of the differential cross sections.

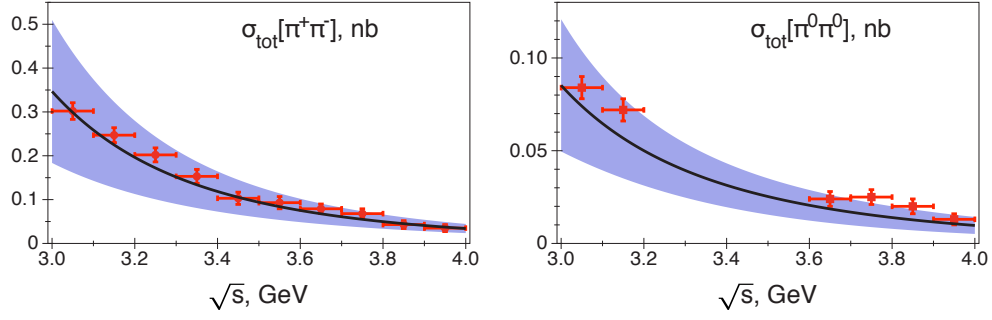


**Figure 18.** The total cross sections as functions of energy.

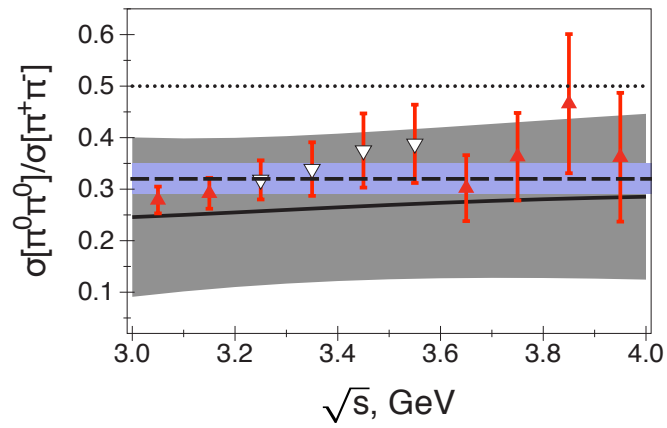


**Figure 19.** The ratio  $\sigma^{\pi^0\pi^0}/\sigma^{\pi^+\pi^-}$  as functions of energy. The notations are the same as in Fig.15.

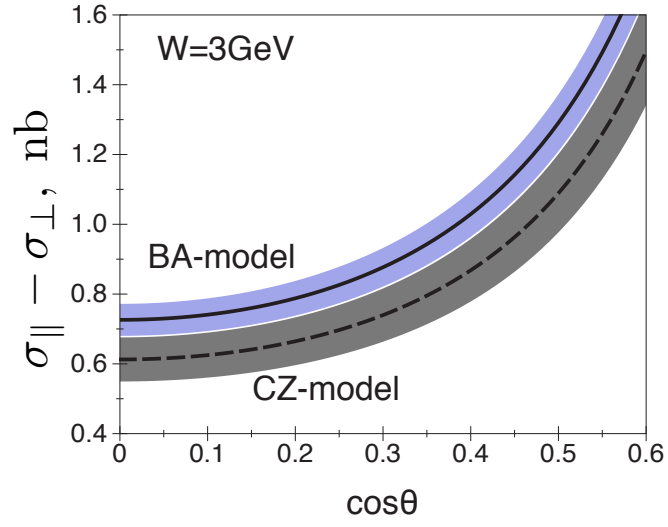


**Figure 20.** Prediction for the combination of the cross sections  $\sigma_{\parallel}^{\gamma\gamma\rightarrow\pi\pi} - \sigma_{\perp}^{\gamma\gamma\rightarrow\pi\pi}$  using the different model of pion DA. See discussion in the text.